Cell Stem Cell

Article

Mitochondrial Potentiation Ameliorates Age-Related Heterogeneity in Hematopoietic Stem Cell Function

Graphical Abstract

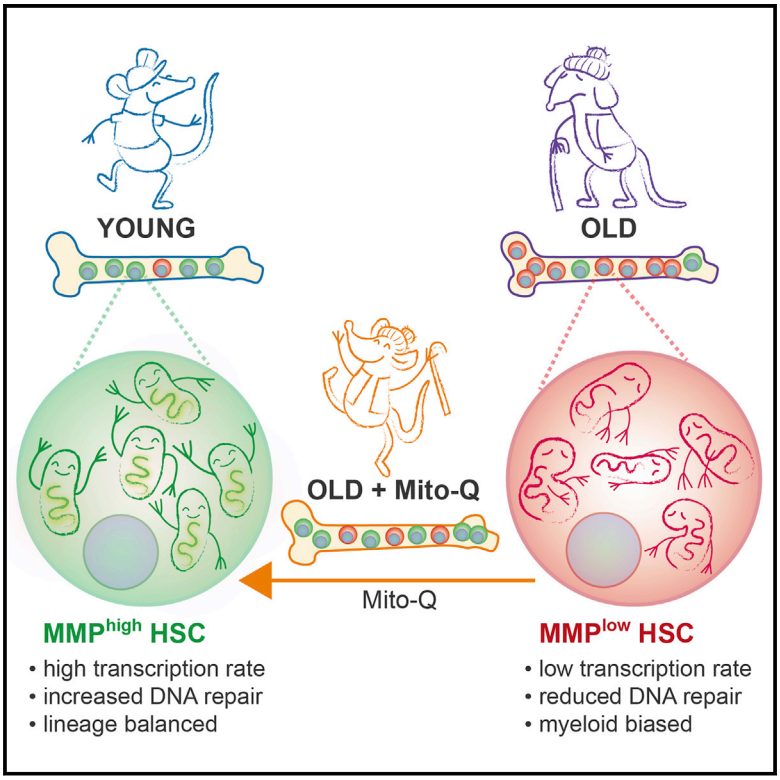

Highlights

- HSCs from old and young mice are heterogeneous for mitochondrial activity (MMP)
- MMP^{high} HSCs from old mice have young-like transcriptional and functional features
- MMP of HSCs can be manipulated *in vivo* with consequences for function
- Mitochondrial potentiation can prevent or ameliorate onset of hematopoietic aging

Authors

Els Mansell, Valgardur Sigurdsson, Elitza Deltcheva, ..., Shamit Soneji, Jonas Larsson, Tariq Enver

Correspondence

els.mansell@med.lu.se (E.M.), t.enver@ucl.ac.uk (T.E.)

In Brief

HSC aging is clinically associated with risk of anemia, immune compromise, and malignancy. Mansell et al. show that mitochondrial activity is directly linked to age-related performance of HSCs and that its perturbation has direct consequences for HSC function, resulting in alleviation or prevention of hematopoietic aging.

Mansell et al., 2021, Cell Stem Cell *28*, 1–16
February 4, 2021
https://doi.org/10.1016/j.stem.2020.09.018

CellPress

Cell Stem Cell

CellPress
OPEN ACCESS

Article

Mitochondrial Potentiation Ameliorates Age-Related Heterogeneity in Hematopoietic Stem Cell Function

Els Mansell,[1,2,*] Valgardur Sigurdsson,[1] Elitza Deltcheva,[2] John Brown,[2] Chela James,[2] Kenichi Miharada,[1] Shamit Soneji,[3] Jonas Larsson,[1] and Tariq Enver[1,2,4,*]

[1]Molecular Medicine and Gene Therapy, Lund University, 22362 Lund, Sweden
[2]Cancer Institute, University College London, London WC1E 6DD, United Kingdom
[3]Department of Molecular Hematology, Lund University, 22362 Lund, Sweden
[4]Lead Contact
*Correspondence: els.mansell@med.lu.se (E.M.), t.enver@ucl.ac.uk (T.E.)
https://doi.org/10.1016/j.stem.2020.09.018

SUMMARY

Aging is associated with reduced fitness and increased myeloid bias of the hematopoietic stem cell (HSC) compartment, causing increased risk of immune compromise, anemia, and malignancy. We show that mitochondrial membrane potential (MMP) can be used to prospectively isolate chronologically old HSCs with transcriptional features and functional attributes characteristic of young HSCs, including a high rate of transcription and balanced lineage-affiliated programs. Strikingly, MMP is a stronger determinant of the quantitative and qualitative transcriptional state of HSCs than chronological age, and transcriptional consequences of manipulation of MMP in HSCs within their native niche suggest a causal relationship. Accordingly, we show that pharmacological enhancement of MMP in old HSCs *in vivo* increases engraftment potential upon transplantation and reverses myeloid-biased peripheral blood output at steady state. Our results demonstrate that MMP is a source of heterogeneity in old HSCs, and its pharmacological manipulation can alter transcriptional programs with beneficial consequences for function.

INTRODUCTION

Hematopoietic stem cells (HSCs) are a rare population of bone marrow (BM) resident cells that sit at the apex of the hematopoietic hierarchy and are capable of self-renewal and lifelong replenishment of all blood lineages (Orkin and Zon, 2008). HSCs are functionally defined by their capacity to reconstitute long-term multi-lineage hematopoiesis of a recipient (Till and McCulloch, 1961; Szilvassy et al., 1990). Murine HSCs defined "phenotypically" on the basis of cell-surface markers can now be purified, such that 40% of single isolated cells produce long-term multi-lineage reconstitution (Oguro et al., 2013).

However, even the most phenotypically homogeneous HSCs may be heterogeneous in respect of their metabolic, epigenetic, transcriptional, and, therefore, behavioral state. With respect to metabolic state, several studies have linked differences in mitochondrial activity or content to differences in HSC state and fate, including cell-cycle status, lineage potential, and engraftment upon transplantation (Luchsinger et al., 2016; Ito et al., 2016; Liang et al., 2020; Umemoto et al., 2018). Traditionally, such studies reported that HSCs have low mitochondrial membrane potential (MMP) and low mitochondrial mass, and these attributes are supportive of stem cell function (Simsek et al., 2010; Rimmelé et al., 2015; Sukumar et al., 2016; Vannini et al., 2016). Recently, however, a number of studies have shown that HSCs have high mitochondrial mass and MMP compared to committed BM populations, and higher mass and potential equates to greater stem cell function (de Almeida et al., 2017; Bonora et al., 2018; Morganti et al., 2019a; Takihara et al., 2019). The contradictory nature of these results may in part relate to how mitochondrial mass and MMP are measured. Mitochondrial mass and potential can be simply assessed using a range of mitochondrial targeted or cationic fluorescent dyes. However, the cellular expulsion of these dyes through xenobiotic efflux pumps may confound analysis, and "true" readings may be obtained only under conditions where these pumps are blocked by inhibitors such as verapamil (VP). This becomes particularly important in the mitochondrial analysis of HSCs and progenitors that express such efflux pumps to a much higher degree than mature BM populations (Chaudhary and Roninson, 1991; Nordahl et al., 2011; de Almeida et al., 2017; Morganti et al., 2019b).

Conventionally, MMP, which represents the electrical potential and proton gradient across the inner mitochondrial membrane, was thought to simply reflect electrical potential generated through oxidative reactions linked to ATP synthesis. However, HSCs reside in low-oxygen niches and rely primarily on anaerobic glycolysis for energy production during quiescence and self-renewal (Ito and Suda, 2014; Kohli and Passegué,

Please cite this article in press as: Mansell et al., Mitochondrial Potentiation Ameliorates Age-Related Heterogeneity in Hematopoietic Stem Cell Function, Cell Stem Cell (2020), https://doi.org/10.1016/j.stem.2020.09.018

2014). Recent studies have focused on aspects of mitochondrial regulation of stem cells beyond ATP production; mitochondria are signaling organelles involved in calcium homeostasis, lysosomal trafficking, inflammation, cell death, and survival signaling, as well as biosynthetic organelles essential for heme, amino acid, and nucleotide metabolism and epigenetic markers (Snoeck, 2017; Zorova et al., 2018; Luchsinger et al., 2019; Ito et al., 2019; Umemoto et al., 2018). The extent to which these different processes are represented by measurements of MMP in stem cells is not fully understood. Furthermore, studies in cell lines have shown that the rate at which cells transcribe RNA is in part determined by mitochondrial content and membrane potential (das Neves et al., 2010). Interestingly, in contrast to many of the aforementioned roles of mitochondria, the transcriptional rate of HSCs and its relation to mitochondrial activity have not yet been explored.

The role that aging plays in stem cell function is an emerging research topic of interest, in part because of a global demographic shift toward an older population. Aging is accompanied by steady functional decline of a variety of organs and tissues and is also the highest risk factor for cancer development (White et al., 2014). Upon aging of the hematopoietic system, the phenotypic HSC pool expands but collectively displays reduced repopulation capacity, increased clonality, myeloid-biased blood output, and lymphoid and erythroid deficiency (Sudo et al., 2000; Liang et al., 2005; Norddahl et al., 2011; Dykstra et al., 2011; Grover et al., 2016). As a consequence, many hematological disorders such as anemia, adaptive immune compromise, and malignancy are strongly age-associated (Pang et al., 2011).

Conceptually, aging can be considered in two distinct ways: chronological age and physiological age. Chronological age reflects the actual age of the organism, and consequently, all stem cells within an organism will share the same chronological age. Physiological age reflects an age-linked performance characteristic. Cells of the same chronological age may thus map to different physiological ages. This raises the possibility that stem cells in aged mice may be heterogeneous with regard to their physiological age with, for example, an age-related characteristic such as myeloid bias being distributed in a heterocellular fashion in old mice (Beerman et al., 2010; Wahlestedt et al., 2017; Montecino-Rodriguez et al., 2019; Gulati et al., 2019).

Since it has been shown that myeloid bias and reduced regenerative capacity of old HSCs are maintained upon transplantation into young mice, it has been suggested that functional alteration with age predominantly results from cell-autologous changes (Rossi et al., 2005). A number of studies have identified cell-intrinsic mechanisms underlying HSC aging, including DNA damage, cellular senescence, increased reactive oxygen species (ROS) production, and mitochondrial dysfunction (de Haan and Lazare, 2018).

We herein explore the possibility that MMP can be used to identify physiologically young HSCs in chronologically aged mice. We test if the transcriptional and functional states of young and old HSCs correlate directly with MMP and, consequently, if manipulation of MMP *in vivo* may impact on age-related performance. We show that despite the decrease in MMP of aging HSCs at the population level, a fraction of HSCs exist in old mice that are similar in MMP to the bulk of HSCs from young mice, thereby identifying MMP as a source of heterogeneity in chronologically old HSCs. Furthermore, we show that MMP directly determines both the rate of transcription and the nature of gene expression of HSCs in their native niche. Finally, we show that MMP of HSCs from old mice can be pharmacologically enhanced *in vivo* with direct consequences for HSC function, as indicated by increased engraftment potential and balanced lineage output upon transplantation. In a steady-state setting, we show that mitochondrial-targeted treatment of aged mice causes reversal of myeloid-biased peripheral blood output and rescue of lympho-erythroid output, highlighting the translational potential of our findings.

RESULTS

Mitochondrial Activity Is a Source of Heterogeneity in Old and Young HSCs

We compared the mitochondrial activity of old and young HSCs and assessed the extent to which age-related changes in mitochondrial parameters apply to all or only a fraction of HSCs within an organism. Staining for mitochondrial mass (mitotracker green [MTG]) or membrane potential (Tetramethylrhodamine methyl ester [TMRM], DilC1(5), Tetramethylrhodamine ethyl ester [TMRE], and JC-1) in the presence of VP was combined with a panel of cell-surface markers to discriminate between stem, progenitor, and mature compartments in the BM of young and old mice (Figure 1A). In line with published literature, we observed a significant increase in the frequency of immunophenotypic HSCs with age, at the expense of the hematopoietic progenitor cell compartment-1 (HPC1) population (Figure 1A).

We first validated the effect of VP on mitochondrial dye retention in HSCs versus bulk BM cells; the impact of VP has been reported for MTG (Norddahl et al., 2011; de Almeida et al., 2017) and recently for TMRM (Bonora et al., 2018) but not for DilC1(5) and TMRE. In absence of VP, primitive progenitor cells (Lin^- $Sca1^+$ $cKit^+$; LSK) and HSCs in particular appear to have lower MMP than committed BM populations (Lin^+) in both young and old animals (Figure S1A). In contrast to a recent report (Liang et al., 2020), we show that inclusion of VP significantly increases staining intensity of all mitochondrial mass and MMP dyes in HSCs, without affecting total BM staining (Figures 1B, S1B, and S1C); thus, we have used VP throughout our study. In accordance with related studies (de Almeida et al., 2017; Bonora et al., 2018; Takihara et al., 2019; Morganti et al., 2019a), our data confirm that HSCs are indeed high in mitochondrial mass as well as MMP relative to mature BM populations, a trend observed in both young and old mice (Figures 1C and S1D). We also saw a marked reduction of MMP with age in progenitors, most pronouncedly in HSCs (Figures 1D and S1E); however, this was not accompanied by any major change in mitochondrial mass as measured by MTG (Figure 1D) and quantifications of the nuclear to mitochondrial DNA ratio (data not shown), indicating a per-mitochondrial mass decrease in activity in old HSCs.

Assessment of the distribution of MMP values showed that both young and old HSCs are heterogeneous with respect to MMP, and the range of MMP values covered by young and old HSCs is broadly similar (Figure 1E). The difference in average MMP value seen at the population level results from a distribution

Please cite this article in press as: Mansell et al., Mitochondrial Potentiation Ameliorates Age-Related Heterogeneity in Hematopoietic Stem Cell Function, Cell Stem Cell (2020), https://doi.org/10.1016/j.stem.2020.09.018

CellPress
OPEN ACCESS

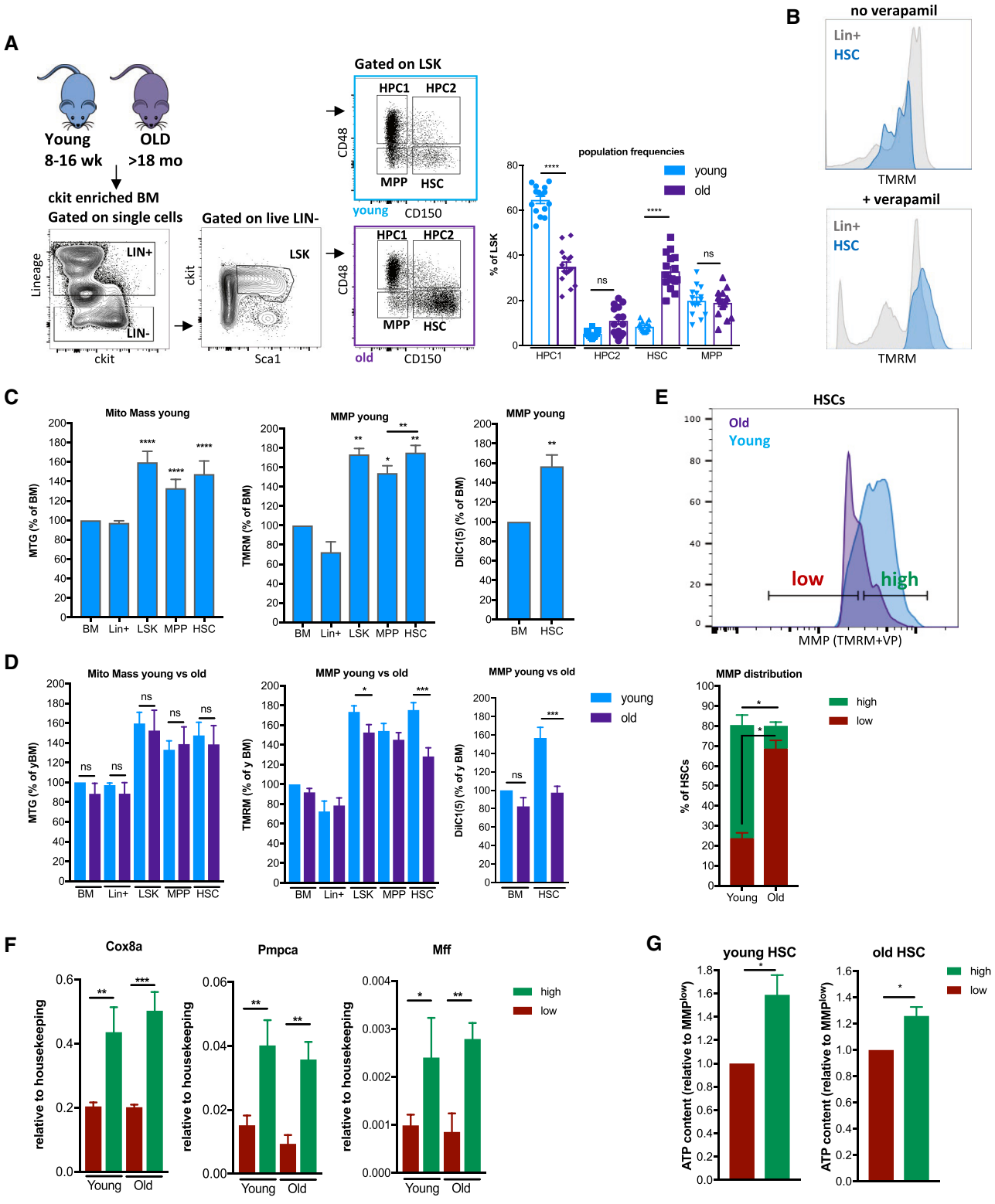

Figure 1. Mitochondrial Activity Is a Source of Heterogeneity in Old and Young HSCs

(A) Left: gating strategy of HSPCs based on signaling lymphocyte activation molecule (SLAM) expression in the lineage (Mac1, Gr1, B220, CD3e, Ter119) Sca1$^+$ c-Kit$^+$ fraction (LSK). Right: frequencies of phenotypic HSCs (CD150$^+$CD48$^-$LSK), multipotent progenitors (MPP, CD150$^-$CD48$^-$LSK), and more restricted progenitor populations HPC1 (CD150$^+$CD48$^-$LSK) and HPC2 (CD150$^+$CD48$^+$LSK) in old and young mice (n = 15).

(B) Representative FACS plots of MMP in HSCs (blue) and Lin$^+$ (gray) cells, as measured by TMRM in absence (top) or presence (bottom) of VP.

(legend continued on next page)

Please cite this article in press as: Mansell et al., Mitochondrial Potentiation Ameliorates Age-Related Heterogeneity in Hematopoietic Stem Cell Function, Cell Stem Cell (2020), https://doi.org/10.1016/j.stem.2020.09.018

shift of old HSCs toward the lower end of this range, while young HSCs center toward the higher end. We categorized HSCs as MMP^{high} or MMP^{low} by splitting this range of values into two components centered around the average median staining intensity (MFI) of young and old HSCs combined, while allowing for a gap between high and low that spans at least 15% of each sample. Based on this, the majority of HSCs in young mice are classified as MMP^{high}. In contrast, only 10%–15% of HSCs from old mice are classified as MMP^{high}, with the MMP^{low} fraction representing the majority of HSCs (Figure 1E).

Next, we confirmed that the cells we operationally defined as MMP^{high} by dye staining express high levels of key mitochondrial genes including *Cox8a*, *Pmpca*, and *Mff* (Figures 1F and S1F), validating our assessment of MMP status.

In addition, we explored how MMP relates to other metabolic parameters. Our data reveal that MMP of HSCs positively correlates with their intracellular ATP content (Figure 1G) and inversely correlates with mitochondrial superoxide generation (Figure S1G) and intracellular ROS (Figure S1H) in both young and old mice. This is of particular interest because low ROS levels are known to support long-term HSC function (Ito et al., 2006; Jang and Sharkis, 2007; Le et al., 2016).

In sum, HSCs are heterogeneous for MMP, and a population of MMP^{high} stem cells exists in the old mice that is similar in MMP to the bulk of young HSCs. This raises the possibility that their similarity may extend beyond MMP to a shared cell state and, by extension, to similarity in function.

Mitochondrial Membrane Potential Determines Transcriptional Rate of HSCs

We first assessed cell state through quantitative and qualitative analyses of transcriptional state. We have previously shown in cell lines that MMP contributes to heterogeneity in global RNA transcription rate, generating cell-to-cell variability in otherwise seemingly homogeneous populations (das Neves et al., 2010; Guantes et al., 2015). Here, we explored this relationship in HSCs in the context of their native BM niche using transcription rate as a quantitative measure of transcriptional state.

We measured transcription rate *in vivo*, using click-it chemistry (Kolb et al., 2001) to detect 5-ethynyl uridine (5-EU) incorporation into nascent RNA over a set period post-intraperitoneal injection (Figure 2A). Remarkably, in young mice, hematopoietic stem and progenitor cells (HSPCs) and HSCs in particular are transcribing faster than committed BM lineages (Figures 2B and S2A). Despite fast RNA transcription, young and old HSCs display a low rate of protein translation, as previously reported (Signer et al., 2014; Sigurdsson et al., 2016; Figures 2C and S2B). In accordance with their lower MMP, HSCs and progenitors in old mice display a significantly lower rate of transcription compared to young HSCs (Figures 2D, S2B, and S2C).

Fluorescence-activated cell sorting (FACS) analysis shows that both old and young HSCs are as heterogeneous for transcription rate as they are for MMP (Figures 2E and S2C). Classification of HSCs as transcription rate "fast" (orange) or "slow" (gray) shows that a small percentage of old HSCs exists that transcribes as fast as the bulk of young HSCs (Figure 2E).

To explore the connection between MMP and transcription rate further, we sorted MMP^{low} and MMP^{high} HSPCs after *in vivo* incorporation with labeled 5-EU and analyzed their transcription rate. Our results confirmed that MMP^{high} HSCs transcribe RNA faster than MMP^{low} HSCs in both young and old mice (Figures 2F and S2D). To further validate the similarity between MMP^{high} and transcription rate "fast" HSPCs, gene expression analysis was performed of genes critical to mRNA transcription, such as subunits of RNA polymerase II (RNA Pol II) (*Polr2a,e*) and elongation factor *Ell2*, in MMP^{low} and MMP^{high}sorted HSPCs and HSCs (Figures 2G and S2E). These data show that genes critical to RNA-Pol-II-driven transcription are significantly upregulated in MMP^{high} compared to MMP^{low} sorted cells in both young and old mice, validating this relationship. In contrast, expression of RNA Pol I transcription termination factor 1 (*Ttf1*) does not appear to correlate with MMP.

In vivo treatment with the mitochondrial uncoupler carbonyl cyanide m-chlorophenyl hydrazine (CCCP) resulted in a reduction of MMP (Figure S2F) concomitant with a significant decrease in transcription rate of BM cells including HSCs (Figures 2I and S2G). To address whether transcription rate is directly dependent on MMP, we compared the effect of CCCP with that of conventional RNA Pol inhibitors (Figure 2H). The magnitude of transcription rate decrease resulting from mitochondrial uncoupling is similar to that produced by broad RNA Pol inhibitor Actinomycin-D and comparable concentrations of the RNA-Pol-II-specific inhibitors 5,6-Dichlorobenzimidazole 1-β-D-ribofuranoside (DRB) and Flavopiridol (Figure 2I). Furthermore, gene expression data of HSPCs isolated from CCCP-treated animals reveal specific downregulation of RNA Pol II subunits alongside downregulation of mitochondrial genes (Figure S2H). Our data are consistent with the notion that the global rate of transcription of HSCs in their native niche is both heterogeneous and dependent on mitochondrial activity.

Mitochondrial Activity Separates Transcriptionally Distinct Subsets of HSCs

We next assessed the qualitative transcriptional state of HSCs that differ in MMP through bulk RNA sequencing. MMP^{high} and MMP^{low} HSCs were sorted from young and old mice as

(C) Analysis of mitochondrial mass (MTG; left) and potential (TMRM; middle and DilC1(5); right) in total BM, committed cells (Lin+), and progenitors (LSK), including MPPs and HSCs in young mice (n = 5).
(D) Comparison of mitochondrial mass (MTG; left) and potential (TMRM; middle and DilC1(5); right) between young (blue) and old (purple) BM lineages, normalized to yBM (n = 5).
(E) Representative FACS plot (top) of MMP values of young (blue) and old (purple) HSCs including analysis of the percentage distribution (bottom) of young and old HSCs that fall into the MMP^{high} (green) and MMP^{low} (red) categories (n = 5).
(F) mRNA expression of *Cox8a*, *Pmpca* and *Mff* in young and old LSK cells sorted according to MMP, normalized to expression of *B2m* (n = 3).
(G) Measurement of ATP content in the 30% MMP^{lowest}- and $MMP^{highest}$-sorted HSCs from young and old (20–24 months) mice (n = 5/6, paired t test).
Results are represented as mean ± SEM. *p < 0.05; **p < 0.01; ***p < 0.001; ****p < 0.0001.

Please cite this article in press as: Mansell et al., Mitochondrial Potentiation Ameliorates Age-Related Heterogeneity in Hematopoietic Stem Cell Function, Cell Stem Cell (2020), https://doi.org/10.1016/j.stem.2020.09.018

CellPress
OPEN ACCESS

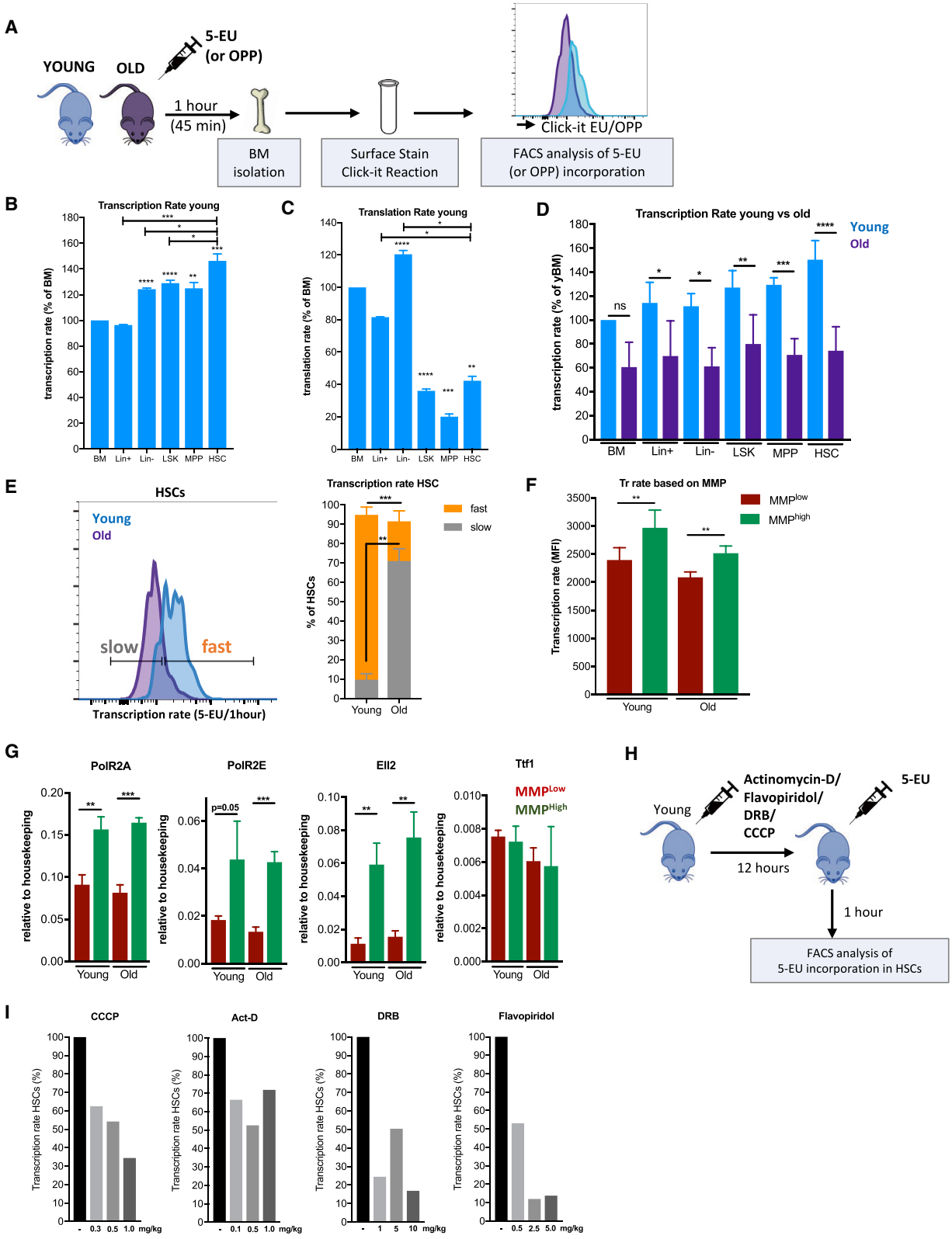

Figure 2. Mitochondrial Membrane Potential Determines Transcriptional Rate of HSCs

(A) Schematic diagram of *in vivo* measurements of transcription (5-EU) and translation (O-propargyl-puromycin; OPP) rate.

(B) *In vivo* transcription rate measurements of BM lineages in young mice normalized to BM (n = 5).

(legend continued on next page)

Please cite this article in press as: Mansell et al., Mitochondrial Potentiation Ameliorates Age-Related Heterogeneity in Hematopoietic Stem Cell Function, Cell Stem Cell (2020), https://doi.org/10.1016/j.stem.2020.09.018

described in Figure 1, albeit enhancing the separation between high and low to span 30% of each sample (Figure 3A).

Using gene set enrichment analysis (GSEA), we validated that MMP^{high} and MMP^{low} HSCs appropriately reflect their mitochondrial state at the transcriptional level (Figures 3B and S3A). Additionally, old HSCs are enriched for age-associated gene expression signatures (Figure S3B, purple box), while young HSCs show higher expression of certain lymphoid lineage-associated genes (Figure S3B, blue box), although expression of some of these genes is also clearly influenced by MMP status (Figure S3B, black box).

Principal-component analysis (PCA) reveals that HSCs group predominantly by MMP rather than by chronological age (Figure 3C). Approximately 1000 genes are significantly differentially expressed between MMP^{high} and MMP^{low} HSCs irrespective of their donor age (Figure 3D). Closest-neighbor analysis (Figure 3E) shows that more genes are differentially expressed between MMP^{high} and MMP^{low} HSCs, irrespective of donor age, than between young and old HSCs, irrespective of their MMP. Overall, this suggests that MMP is a greater determinant of transcriptional state than chronological age, and while old HSCs as a population are broadly transcriptionally distinct from their younger counterparts, a fraction do share significant transcriptional similarity with young HSCs, and these may be identified through MMP.

We next explored the underlying basis of transcriptional similarity of cells sharing the same MMP. GSEA (Figures 3F and S3C) reveals an age-related signature associated with low MMP, exemplified by upregulation of inflammatory signaling and apoptotic pathways and downregulation of DNA repair pathways (Nijnik et al., 2007; Rossi et al., 2007; Kirschner et al., 2017). Critically, upregulation of inflammation and downregulation of DNA repair are drivers of oncogenesis, relevant perhaps to the strong age dependency of leukemia (Akunuru and Geiger, 2016). GSEA also shows that MMP^{high} HSCs are enriched for pathways linked to transcriptional rate, including purine and pyrimidine metabolism, RNA turnover, and spliceosome pathways.

Furthermore, GSEA comparing our raw dataset to published lineage signatures (Novershtern et al., 2011) reveals that MMP^{low} HSCs are enriched for granulocyte and monocyte progenitor (GMP) signatures and downregulation of erythroid, early erythroid, Pro-B, and early T cell programs, compared to MMP^{high} HSCs (Figures 3F and S3C). For a more global assessment of lineage in relation to MMP, we used CellRadar, which compares selected gene sets to published lineage-associated genes. These data show that MMP^{low} HSCs are primarily enriched for granulocyte, monocyte, and long-term HSC (LT-HSC) signatures (Figure 3G) in a manner nearly identical to CellRadar analyses of genes upregulated upon HSC aging (Figure 3H). Genes upregulated in MMP^{high} HSCs, in contrast, reveal a more diverse lineage pattern covering numerous lymphoid, erythroid, and mixed-lineage precursor populations (Figure 3G) in a manner more closely resembling CellRadar analyses of genes upregulated in young HSCs (Figure S3D).

Finally, we tested the connection between MMP and lineage using a literature-derived candidate gene approach (Rossi et al., 2005; Challen et al., 2010); age-associated genes with implications for myeloid or platelet bias are nearly exclusively upregulated in MMP^{low} HSCs, whereas genes involved in lymphoid and erythroid priming are found to be upregulated in MMP^{high} HSCs (Figures 3D and S3E).

We conclude from these data that MMP separates HSCs with quantitatively and qualitatively distinct transcriptional states, irrespective of chronological age. Furthermore, sorting cells based on low and high MMP segregates the transcriptional changes that are characteristic of old and young HSCs, respectively.

In Vivo Manipulation of MMP Alters the Transcriptional States of HSCs

To see if MMP is a functional determinant of transcriptional state, we next experimentally manipulated MMP levels of HSCs *in vivo* (Figure 4A). We both uncoupled the mitochondrial respiratory chain by injection of CCCP (Figure 2H) and enhanced MMP using mitoquinol (Mito-Q), a mitochondrial-targeted coenzyme-Q10 (Murphy and Smith, 2007), which successfully increased MMP of old HSCs *in vitro* (Figure S4A). We show that successive Mito-Q injection significantly enhanced the MMP of old HSCs in their native niche (Figures 4B and S4B), increased their global rate of transcription (Figures 4B and S4C), and decreased their levels of intracellular ROS (Figure S4D).

Mito-Q treatment of old mice caused a significant frequency shift from HSCs to the HPC1 fraction, thereby partially restoring the skewed distribution of HSPCs (Figure 4C) normally seen in aged animals (see Figure 1A). CD150 expression has been used to distinguish between predominantly lymphoid-biased (Ly; CD150^{low}) and myeloid-biased (My; CD150^{high}) HSCs, the latter becoming dominant with age (Beerman et al., 2010; Figures 4C and 4D). Interestingly, short-term Mito-Q treatment causes a significant increase in Ly-HSCs at the expense of My-HSCs (Figure 4D) through selective cycling of Ly-HSCs (Figures 4E and S4E). These changes are in line with our observation that Ly-HSCs have higher MMP than My-HSCs (Figure S4F). Collectively these results show that a 5-day treatment of old mice with Mito-Q causes phenotypic changes in HSCs that are

(C) *In vivo* protein translation rate measurements of BM lineages in young mice normalized to BM (n = 4).
(D) Comparison of transcription rate between young (blue) and old (purple) BM lineages, normalized yBM (n = 5).
(E) Representative FACS plot of transcription rate of young (blue) and old (purple) HSCs (left) including analysis of the percentage distribution (right) of young and old HSCs that fall into the transcription rate^{fast} (orange) and transcription rate^{slow} (gray) categories (n = 5).
(F) Transcription rate analysis in the 30% MMP^{lowest}- and MMP^{highest}-sorted HSCs from young or old (18–24 months) mice (n = 9 [Y], n = 5 [O]). Ratio paired t test.
(G) mRNA expression of RNA Pol II subunits *Polr2a*, *Polr2e*, and elongation factor *Ell2*, as well as RNA Pol I transcription termination factor 1 (*Ttf1*) in young and old LSK cells sorted by MMP, normalized to expression of *B2m* (n = 3).
(H) Schematic diagram of experimental procedure.
(I) Transcription rate in HSCs after *in vivo* treatment with mitochondrial uncoupler CCCP compared to RNA Pol inhibitors Actinomycin-D, DRB, and Flavopiridol at three concentrations. (n = 1 per concentration).
Results are represented as mean ± SEM. *p < 0.05; **p < 0.01; ***p < 0.001; ****p < 0.0001.

Please cite this article in press as: Mansell et al., Mitochondrial Potentiation Ameliorates Age-Related Heterogeneity in Hematopoietic Stem Cell Function, Cell Stem Cell (2020), https://doi.org/10.1016/j.stem.2020.09.018

CellPress
OPEN ACCESS

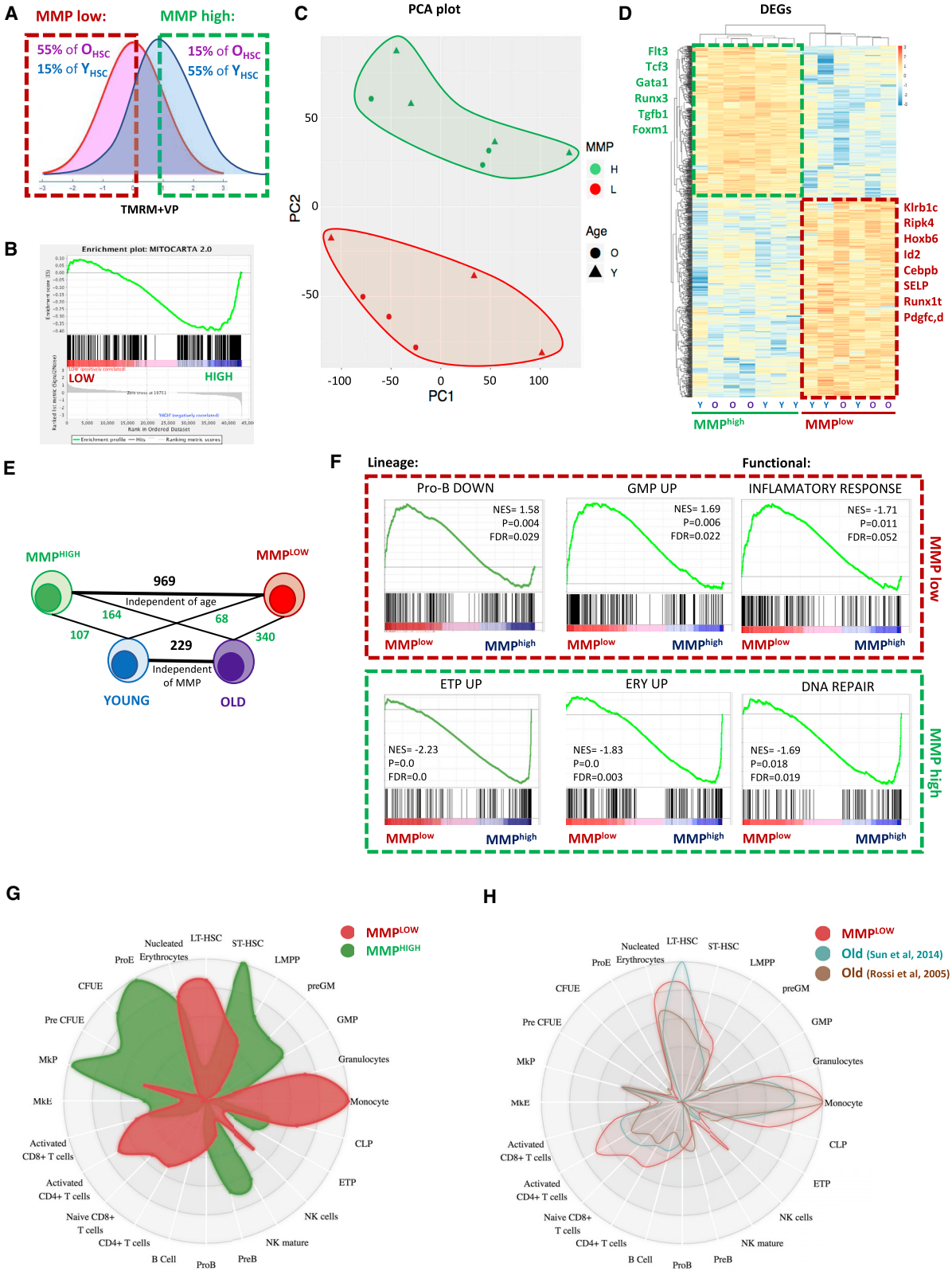

(legend on next page)

Please cite this article in press as: Mansell et al., Mitochondrial Potentiation Ameliorates Age-Related Heterogeneity in Hematopoietic Stem Cell Function, Cell Stem Cell (2020), https://doi.org/10.1016/j.stem.2020.09.018

suggestive of a change in functional state, with the possible caveat that Mito-Q treatment may affect cell-surface marker expression.

We therefore assessed whether increasing the MMP of old HSCs toward values observed in young HSCs would increase their transcriptional similarity to young HSCs and vice versa. RNA sequencing was performed on HSCs isolated from old untreated animals (O), old Mito-Q-treated animals (O+MQ), young untreated animals (Y), and young CCCP-treated animals (Y-CCCP) (Figure 4A).

Interestingly, PCA reveals that old HSCs isolated from Mito-Q-treated animals show greater transcriptional similarity to young HSCs than to old HSCs from untreated animals (Figure S4G). We next grouped samples into "higher MMP," consisting of young untreated HSCs and old HSCs with enhanced MMP through Mito-Q treatment, and "lower MMP," consisting of old untreated HSCs and young HSCs after mitochondrial uncoupling through CCCP (Figure 4F). We then identified commonly upregulated and downregulated genes in higher MMP compared to lower MMP HSCs, irrespective of donor age (Figure 4G). In parallel, we compared all old samples to all young samples, irrespective of treatment. More genes are differentially expressed between higher MMP and lower MMP samples, irrespective of donor age, than between old and young samples, irrespective of treatment (Figure 4F). While the transcriptional state change effected by manipulation of MMP is not complete, our data suggest that the MMP of HSCs, whether naturally occurring or achieved through *in vivo* pharmacological manipulation, is a bigger determinant of transcriptional state than is the age of the donor mice.

We next explored the nature of genes that are commonly up- or downregulated in both old Mito-Q-treated and young untreated HSCs to assess if the transcriptional state change in response to Mito-Q is suggestive of a functional state shift. The differentially expressed genes (DEGs) that are significantly upregulated in higher MMP samples irrespective of chronological age comprise many genes that are critical for HSC function and self-renewal, including many transcription factors (TFs) (Figure 4H). Furthermore, Gene Ontology analysis reveals that the top upregulated pathways that are shared between young untreated and old Mito-Q-treated HSCs are highly representative of increased transcriptional rate and also include upregulation of DNA repair pathways (Figure 4H). We functionally validated the increased DNA repair capacity of old HSCs after Mito-Q treatment through measurements of DNA double-strand breaks (marked by γ-H2AX) after 2 Gy of irradiation. We show that HSCs, but not bulk BM, from old Mito-Q-treated mice have significantly reduced levels of DNA damage after irradiation compared to HSCs from old untreated mice, despite no difference in γ-H2AX levels at steady state (Figure S4H). Similar results are obtained upon short-term *ex vivo* treatment with Mito-Q of HSCs that were exposed to irradiation *in vivo* (Figure S4I).

Furthermore, CellRadar indicates that these DEGs are relevant to lineage (Figure 4I): higher MMP correlates with increased lymphoid programming, reflected in signatures for lymphoid-primed multipotent progenitors (LMPPs), early T cell progenitors (ETPs), natural killer cells (NKs), and both pre-and pro-B cell lineages. These signatures are absent in the CellRadar profiles of both old untreated and MMP^{low}sorted HSCs (Figures 4I and 3H). The CellRadar plot based on genes that are upregulated in old Mito-Q-treated versus old untreated HSCs is nearly identical in shape to the CellRadar plot based on genes that are upregulated in young compared to young uncoupled HSCs, suggesting that this lineage signature is specific to elevated MMP of HSCs from both young and old animals.

Our data thus suggest that changing MMP acts directly on the level of stem cells to change their qualitative and quantitative transcriptional state, as well as the balance between lymphoid- and myeloid-biased stem cells. The nature of change in old HSCs upon Mito-Q treatment reveals greater transcriptional similarity with young HSCs that extends to pathways highly relevant to stem cell fitness and lineage output, thus suggesting that this transcriptional state change might be accompanied by a functional state change.

HSCs from Mito-Q-Treated Old Mice Display Superior Engraftment and Lineage Kinetics upon Transplantation

To assess the extent to which HSC function is intrinsically altered upon Mito-Q treatment, we performed competitive transplantation assays. Three hundred HSCs isolated from old Mito-Q-treated mice (O+MQ, according to Figure 4A) or from old untreated mice (O) were competitively transplanted against 100 HSCs from young mice (Y) together with 200,000 BM support cells into lethally irradiated mice. Since recipient mice were never exposed to Mito-Q, any difference in readout would result from intrinsically sustained changes in old HSCs that were treated *in vivo* prior to isolation and transplantation. Peripheral blood (PB) engraftment was monitored until the 16-week endpoint, when BM engraftment was also analyzed (Figure 5A).

First, we assessed if the MMP of HSCs that are transplanted influences the MMP of their progeny. We observed that young donor HSCs reconstitute BM, which, 16 weeks after

Figure 3. Mitochondrial Activity Separates Transcriptionally Distinct Subsets of HSCs

(A) Sorting strategy.

(B) GSEA plot comparing raw sequencing data of MMP^{low} versus MMP^{high} HSCs irrespective of donor age with the top 500 genes from the mouse Mitocarta2.0 list.

(C) PCA of MMP^{high} (H, green) and MMP^{low} (L, red) sorted HSCs from young (Y, triangle) and old (O, circle) mice.

(D) Heatmap of DEGs (FC > 2, FDR < 5%) between MMP^{low} and MMP^{high} HSCs irrespective of donor age, highlighting known lineage-bias genes (Rossi et al., 2005; Challen et al., 2010).

(E) Distance to neighbor analysis plotting number of DEGs (black) as a distance between populations. Overlap of DEGs between young and old and a certain MMP state are shown in green, where greater overlap represents closeness.

(F) Examples of significantly up- or downregulated pathways associated with low or high MMP based on GSEA. Further analysis in Figure S3C.

(G) CellRadar plot comparing genes significantly upregulated in MMP^{low} HSCs and MMP^{high} HSCs irrespective of donor age.

(H) CellRadar plot of genes significantly upregulated in MMP^{low} HSCs irrespective of donor age against genes that are significantly upregulated in old versus young HSCs according to literature.

Please cite this article in press as: Mansell et al., Mitochondrial Potentiation Ameliorates Age-Related Heterogeneity in Hematopoietic Stem Cell Function, Cell Stem Cell (2020), https://doi.org/10.1016/j.stem.2020.09.018

CellPress
OPEN ACCESS

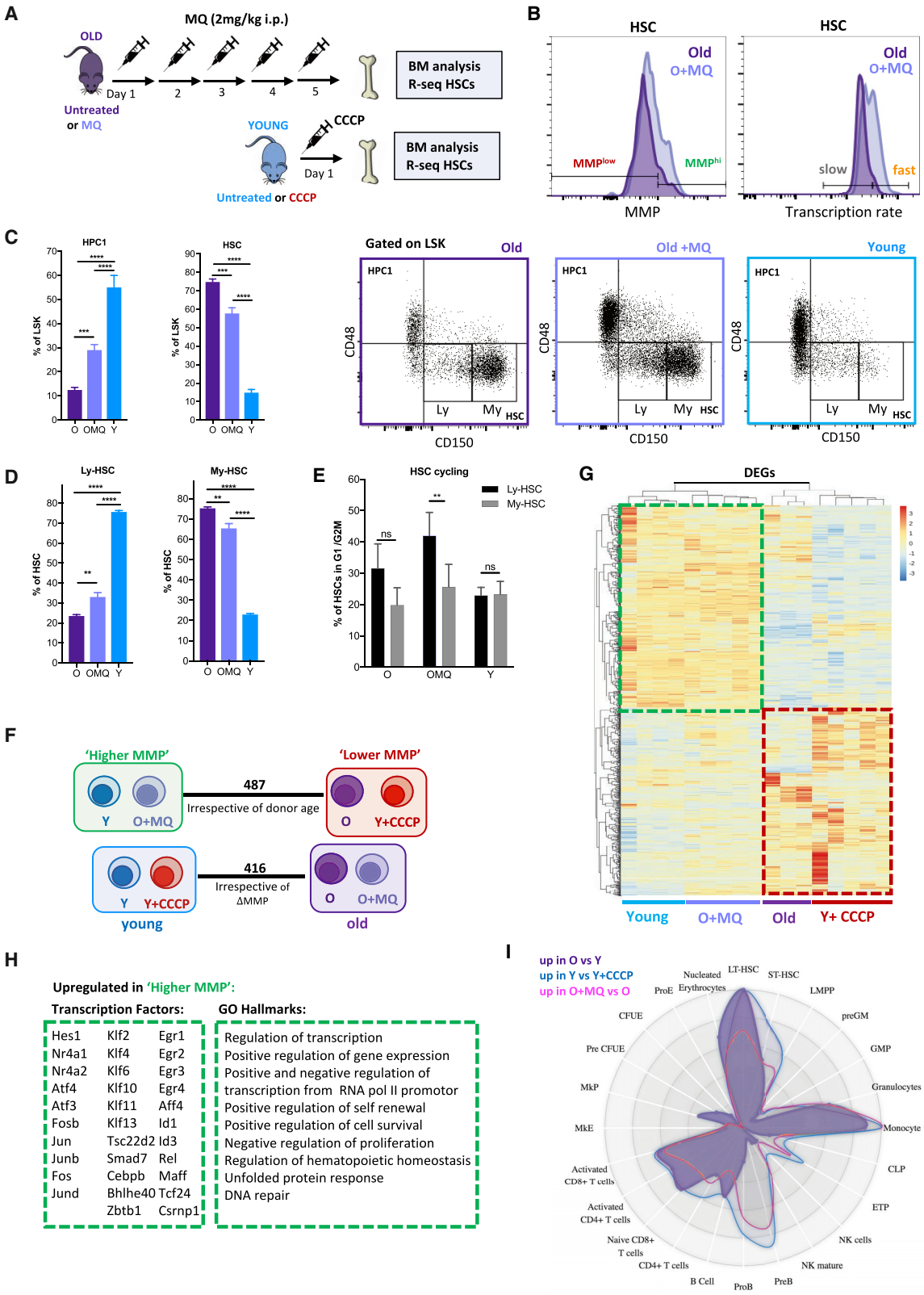

Figure 4. *In Vivo* Manipulation of MMP Alters the Transcriptional States of HSCs

(A) Strategy of *in vivo* modulation of MMP in old (purple) and young (blue) mice using Mito-Q or CCCP.

(B) Representative FACS plots of MMP (left) and transcription rate (right) in old HSCs after Mito-Q (lilac) compared to old control HSCs (purple).

(legend continued on next page)

Please cite this article in press as: Mansell et al., Mitochondrial Potentiation Ameliorates Age-Related Heterogeneity in Hematopoietic Stem Cell Function, Cell Stem Cell (2020), https://doi.org/10.1016/j.stem.2020.09.018

transplantation, shows a similar trend in MMP values across lineages as observed in young mice at steady state (Figures 5B and 1C). Old donor HSCs reconstitute lineages that are lower in MMP than lineages derived from young donor HSCs (Figures 5B and S5A). Interestingly, BM reconstituted by old Mito-Q-treated donor HSCs has significantly higher MMP than BM derived from old untreated donor HSCs and is similar in MMP to BM reconstituted by young HSCs (Figures 5B and 5C). Moreover, both old Mito-Q-treated and young HSCs reconstitute a stem cell pool that is higher in MMP compared to the HSC pool derived from old untreated donors (Figures 5C and S5B).

Importantly, analysis of the kinetics of reconstitution revealed that old HSCs isolated from Mito-Q-treated mice showed significantly superior PB engraftment compared to old untreated HSCs (Figure 5D). Old HSCs from Mito-Q-treated mice also show improved lineage kinetics, producing significantly more B cells than old HSCs from untreated mice, together with a quicker reduction of myeloid-biased output (Figure 5D). BM engraftment 16 weeks after transplantation reflects the blood observations (Figures 5E and 5F), with a nearly 2-fold-greater engraftment from HSCs derived from Mito-Q-treated old mice compared to untreated old mice (Figure 5E). Further analysis revealed that O+MQ HSCs perform equally well as their competitors, consisting of both young HSCs and support BM, whereas old untreated HSCs are significantly outcompeted by their competitors (Figures 5E and S5C).

Thus, the transcriptional state change in old HSCs in response to mitochondrial potentiation is accompanied by increased engraftment potential, improved B cell output, and reduced myeloid bias and suggests that the effect of short-term *in vivo* Mito-Q treatment on HSCs is cell intrinsic and, intriguingly, can be maintained upon stem cell transplantation with long-term consequences for function.

Mito-Q Treatment Can Both Revert and Prevent Onset of the Hematopoietic Aging Phenotype

Since stem cell behavior in a homeostatic setting may be distinct from that seen in a transplant (Busch and Rodewald, 2016; Rodriguez-Fraticelli et al., 2018; Säwen et al., 2018), we next tested the activity of Mito-Q on hematopoiesis at steady state by asking whether it could revert or prevent the onset of hematopoietic aging, thereby assessing its translational potential in the amelioration or prevention of age-related blood disorders.

We measured PB parameters before, during, and after 5 days of treatment of old mice with Mito-Q (Figure 6A) using correction of myeloid bias and rescue of lymphoid output as a measure of functional improvement. Because the trajectory of aging varies from mouse to mouse, resulting in a cohort of 18-month-old mice with different age-related phenotypes, we individually monitored mice receiving Mito-Q. Strikingly, every old Mito-Q-treated animal shows reduction in myeloid output between the start and end of treatment, in the magnitude of 2% to 46% (Figure 6B). This is accompanied by an increased output of B cells of up to 34% seen in all but one individual (Figure 6C). Qualitative changes in B cells were also evident, as shown by a proportionate increase in Immunoglobulin-M expressing (IgM^+) B cells (Figures 6D and S6A). Upon Mito-Q treatment, myeloid and B cell output have significantly changed compared to old untreated mice to such an extent that they are no longer significantly different from young mice (Figure 6E). Mito-Q treatment also caused a significant increase in T cells (Figure S6B). Importantly, the proportional changes in lymphoid versus myeloid output occurred without changing total blood counts (Figure 6F). Of note, treatment of young mice with Mito-Q did not alter PB parameters (data not shown).

We extended these findings in a smaller cohort of young and old mice treated with or without Mito-Q in their drinking water for a period of 10 weeks to assess the utility of Mito-Q delivered in a manner more compatible with any potential therapeutic use (Figure S6C). Adding Mito-Q to the drinking water of old mice produced similar changes in myeloid, lymphoid, and erythroid kinetics (Figures S6D–S6F) to direct Mito-Q injection. Supplementing the drinking water of young mice for 10 weeks did not significantly affect blood and BM parameters.

These results further raise the possibility that earlier intervention might prevent or attenuate the onset of an aging phenotype. To test this, we supplemented the drinking water of 14-month-old middle-aged (MA) mice without (O) or with Mito-Q (OMQ), monitoring the ratio of myeloid to B cells of individual mice over 5 months (Figure 6G). Mice that had Mito-Q-supplemented water have a similar ratio of myeloid to B cells in the PB as MA mice at the start of the experiment, whereas naturally aged mice developed significant myeloid bias (Figures 6H and S6G). Accordingly, 19-month-old mice that aged with Mito-Q water have significantly more B cells and fewer myeloid cells than naturally aged mice (Figure 6H). Again, these changes occurred without affecting total white blood cell counts (Figure S6H). Critically, Mito-Q treatment also prevented onset of anemia that occurred with natural aging, as evidenced by the significant increase in red blood cell count, hemoglobin, and hematocrit of mice that received Mito-Q water

(C) Left: frequencies of HSCs and HPC1 in old (purple), young (blue), and old mice after 5 days of Mito-Q treatment (lilac). Right: representative SLAM FACS plots (n = 7 [O], n = 9 [OMQ], n = 5 [Y]).
(D) Quantification of lymphoid- (Ly) and myeloid- (My) biased HSCs, based on CD150 expression, in old (purple), old Mito-Q-treated (lilac), or young (blue) mice (n = 4).
(E) Percentage of cycling HSCs (in G1/G2M phase) based on CD150 expression (Ly-HSC, black; My-HSC, gray) in old, old Mito-Q-treated, or young mice (n = 4).
(F) Distance to neighbor analysis grouping HSC samples either by their MMP (top) or by chronological age (bottom), using number of DEGs as a measure of distance.
(G) Heatmap of DEGs (FC > 2, FDR < 10%) commonly up- or downregulated between young HSCs and HSCs from old Mito-Q-treated mice (blue and lilac, left) compared to old HSCs and young HSCs from CCCP-treated mice (purple and red, right).
(H) Left: all transcription factors (TFs) that are commonly upregulated in "higher MMP" samples compared to "lower MMP" samples (F). Right: Gene Ontology analysis of DEGs that are upregulated in higher MMP HSCs.
(I) CellRadar plot indicating the lineage potential that correspond with old age (purple) compared to lineage potential associated with higher MMP of HSCs from young (blue) or old (pink) mice.
Results are represented as mean ± SEM. **p < 0.01; ***p < 0.001; ****p < 0.0001.

Please cite this article in press as: Mansell et al., Mitochondrial Potentiation Ameliorates Age-Related Heterogeneity in Hematopoietic Stem Cell Function, Cell Stem Cell (2020), https://doi.org/10.1016/j.stem.2020.09.018

CellPress
OPEN ACCESS

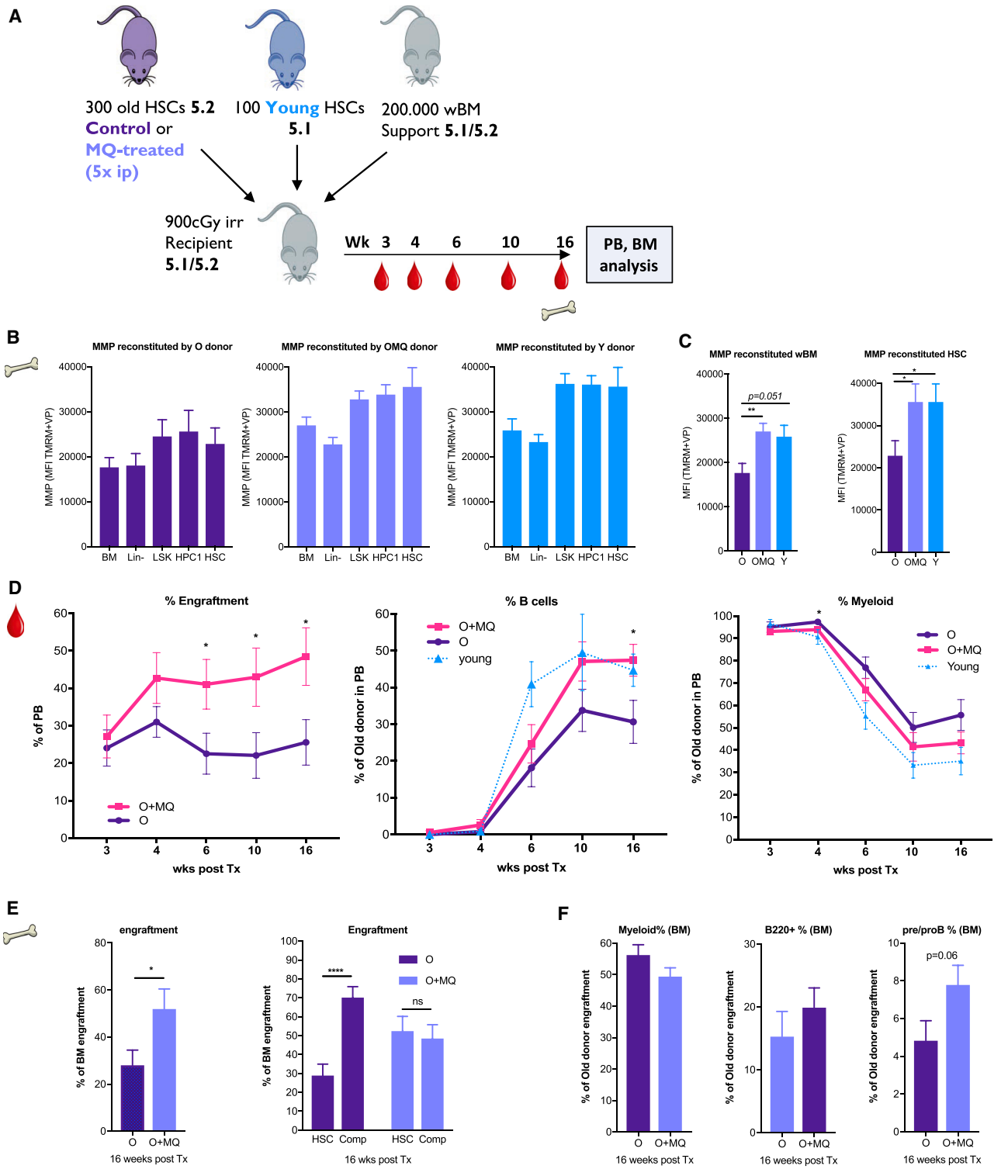

Figure 5. HSCs from Mito-Q-Treated Old Mice Display Superior Engraftment and Lineage Kinetics upon Transplantation

(A) Transplantation setup.

(B) FACS analysis of MMP (TMRM+VP) in BM lineages retrieved 16 weeks after transplantation, separated based on donor origin. Left: derived from old untreated donor HSCs (n = 10); middle: derived from old Mito-Q-treated donor HSCs (n = 9); right: young HSC donor derived (n = 21).

(C) Comparison of MMP in BM (left) or HSCs (right) 16 weeks after transplantation, reconstituted by old untreated donor HSCs (purple, n = 10), old HSCs from Mito-Q-treated donors (lilac, n = 9), or young donor HSCs (blue, n = 21).

(legend continued on next page)

Please cite this article in press as: Mansell et al., Mitochondrial Potentiation Ameliorates Age-Related Heterogeneity in Hematopoietic Stem Cell Function, Cell Stem Cell (2020), https://doi.org/10.1016/j.stem.2020.09.018

for 5 months (Figure 6I). Mirroring the PB observations, BMs of old mice that aged with Mito-Q-supplemented water have a significantly smaller proportion of myeloid cells and a significantly greater proportion of B cells, including the $IgM^{-}B220^{+}$ compartment consisting of pre- and pro-B cells, compared to naturally aged mice (Figure 6J), as well as higher levels of mature erythroid progenitors (Figures 6K and S6I). Additionally, there is a less-exaggerated expansion of phenotypic HSPCs including HSCs when mice age with Mito-Q-supplemented drinking water (Figure S6J).

In sum, Mito-Q supplementation of MA or old mice results, respectively, in the attenuation or partial reversal of an aging phenotype, highlighting the translational potential of our findings.

DISCUSSION

Herein, we have shown that (1) MMP is a source of heterogeneity of old HSCs, with a fraction of old HSCs having similarly high MMP as the bulk of young HSCs; (2) MMP is a bigger determinant of the quantitative and qualitative transcriptional state of HSCs than chronological age; (3) MMP of HSCs can be altered *in vivo*; (4) enhancement of MMP changes the transcriptional landscape of old HSCs, including rescue of lympho-erythroid programs and DNA repair pathways; (5) these transcriptional changes read out as functional improvement in stem cell transplantation assays; and (6) Mito-Q can ameliorate or prevent onset of an aging phenotype.

Age-related changes in hematopoiesis include expansion of phenotypic HSCs, reduced engraftment, and myeloid skewing. While mitochondrial dysfunction has been implicated in aging of the blood system (de Haan and Lazare, 2018), the extent to which age-related phenotypes of HSCs directly result from changes in mitochondrial biology is not fully understood. One study demonstrated that a mouse model of mitochondrial DNA mutagenesis can manifest some aspects of chronological stem cell aging (lineage skewing), but not all (molecular and phenotypic changes) (Norddahl et al., 2011). Of note, MMP was not affected in this mouse model. Our demonstration that Mito-Q treatment causes reversal or stabilization of age-related parameters of the PB and BM addresses this issue directly, and several lines of evidence suggest that these functional changes may be attributed to altering MMP at the level of HSCs. First, short-term Mito-Q treatment directly changes both quantitative and qualitative transcriptional programs at the level of stem cells, including a shift in lineage-affiliated programs, consistent with the rebalancing of lineage output observed in treated mice. Second, Mito-Q treatment corrects the excess representation of phenotypic HSC seen in aged mice and results in selective cycling of lymphoid-biased HSCs at the expense of myeloid-biased HSCs. Lastly, HSCs isolated from Mito-Q-treated old mice are functionally superior to HSCs isolated from untreated old mice upon transplantation into untreated animals, both in respect to total engraftment and lineage distribution of reconstitution. These data highlight that HSCs are intrinsically changed upon short-term Mito-Q treatment with long-term functional consequences. This aside, we do not exclude the possibility that there may be additional and potentially beneficial effects of Mito-Q downstream of stem cells (e.g., stemming from the increased HPC1 fraction harboring LMPPs) when mice receive Mito-Q.

Germane to the issue of chronological versus physiological aging, we conclude that HSCs age in a heterocellular manner, leading to functional heterogeneity in the aged stem cell pool, which may both be dynamic and, importantly, perturbable.

Strikingly, we show that HSCs transcribe RNA quickly, relative to both mature BM and uncommitted progenitor populations. In line with prior cell line studies (das Neves et al., 2010), we show that the transcriptional rate of HSCs correlates with their MMP, and both are significantly decreased in aging HSCs. Remarkably, the rate of transcription changes when MMP is perturbed, suggesting a cause-and-effect relationship. Why a high rate of transcription might be beneficial to stem cells is less clear, but we are intrigued by the possibility that a high transcriptional rate might in some way facilitate high stem cell fate plasticity. In any event, the extent to which transcription rate is or is not related to qualitatively different patterns in gene expression merits further investigation. Interestingly, the high transcriptional rate is not reflected in the rate of protein synthesis. On the contrary, HSPCs are characterized by a significantly lower rate of translation compared to more mature populations, thus suggesting an uncoupling of transcription from protein translation in HSCs at steady state. Such a phenomenon has recently been described in neuronal stem cells (Baser et al., 2019), raising the possibility that this might apply to other multipotent and potentially pluripotent stem cells.

Finally, our experiments that show that age-related parameters in the blood can be reversed under homeostatic conditions, or indeed prevented by the simple addition of Mito-Q to the drinking water, suggest that Mito-Q could be used in a setting where it might offer clinical benefit. Indeed, Mito-Q has been used in clinical trials of neurodegenerative diseases such as Alzheimer's disease, multiple sclerosis and Parkinson's disease, liver pathologies, and kidney and cardiovascular disease, and registered trials in the recruitment phase also involve the musculoskeletal system, platelet function, and asthma (Jin et al., 2014; Kumar and Singh, 2015; Rossman et al., 2018; Ribeiro et al., 2018). With respect to the blood system, we speculate that possible situations in which mitochondrial potentiation may be worth considering include autologous stem cell transplantation in elderly patients receiving high-dose chemotherapy and anemia of the elderly. Furthermore, MMP^{low} HSCs that become abundant with age are characterized by myeloid skewing, upregulation of ROS and inflammatory pathways, and downregulation of DNA repair programs, all of which are predisposing factors to clonal diseases such as myelodysplastic syndrome (MDS) that primarily

(D) Total PB engraftment in recipients receiving old untreated HSCs (purple) or old HSCs from Mito-Q-treated mice (pink) (left) as well as analysis of B cell engraftment (middle) and myeloid engraftment (right), compared to kinetics of young co-transplanted HSCs (blue, dotted) (n = 9–14).

(E) Total BM engraftment (left) and relative contribution of old donor HSC compared to competitor cells (right) (n = 10–13).

(F) Myeloid, B cell, and pre-/pro-B cell percentages of BM engraftment from old untreated (purple) or HSCs from old Mito-Q-treated (lilac) mice 16 weeks after transplantation (n = 10–13).

Results are represented as mean ± SEM. *p < 0.05; **p < 0.01; ****p < 0.0001.

Please cite this article in press as: Mansell et al., Mitochondrial Potentiation Ameliorates Age-Related Heterogeneity in Hematopoietic Stem Cell Function, Cell Stem Cell (2020), https://doi.org/10.1016/j.stem.2020.09.018

CellPress
OPEN ACCESS

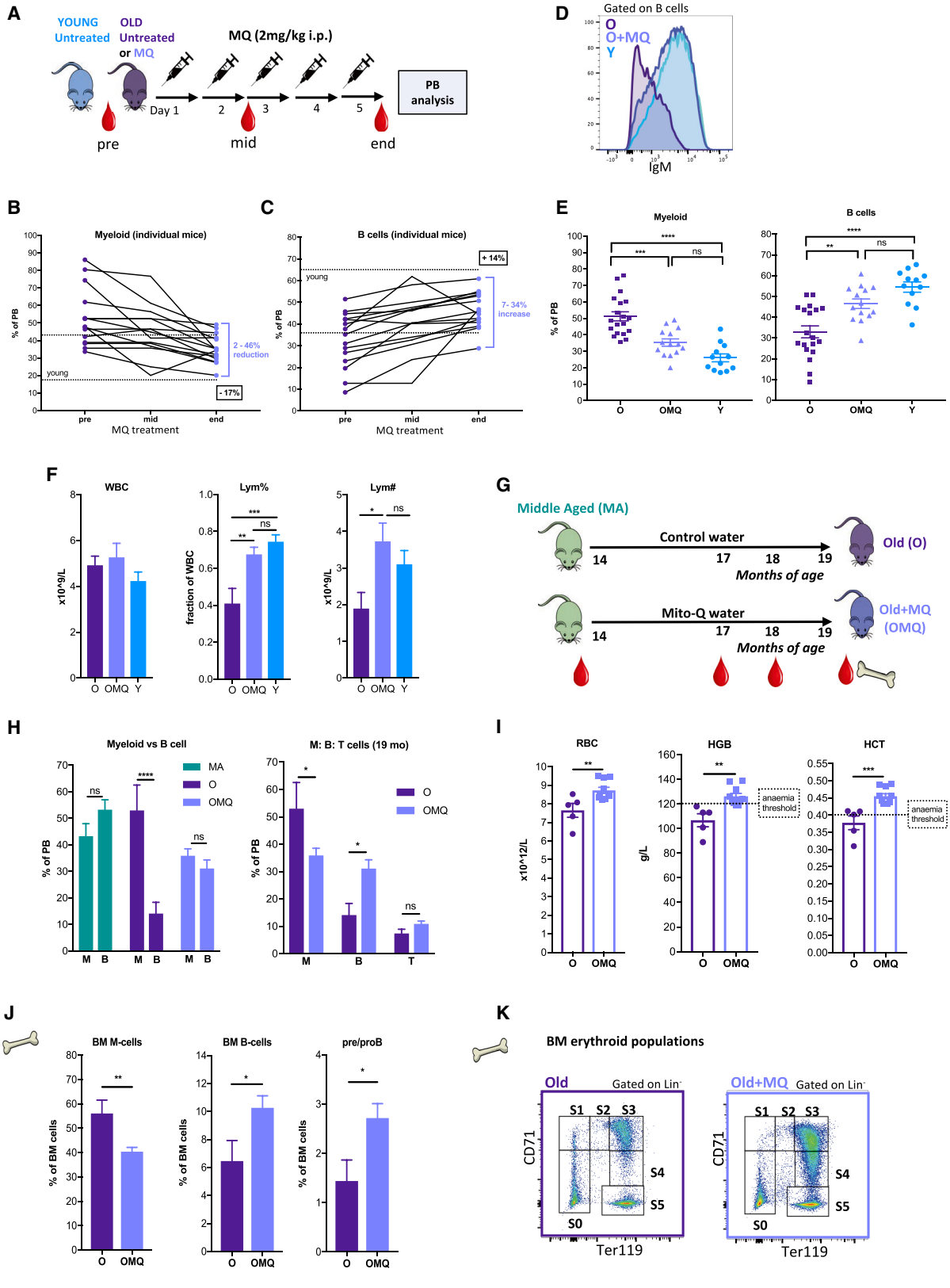

(legend on next page)

affect patients of advanced age. Given the fact that Mito-Q at least partly resolves these age-related features at the stem cell level, we speculate that it may have a role in the prevention of age-related clonal diseases such as MDS.

Limitations of the Study

As mentioned earlier, analysis of MMP in HSCs is confounded by expulsion of mitochondrial dyes unless cellular efflux pumps are inhibited by VP, potentially accounting for conflicting published reports. We, like other recent studies (de Almeida et al., 2017; Takihara et al., 2019; Morganti et al., 2019a), observe that the MMP^{high} fraction is enriched for stem cell potential. Our transcriptional analyses confirm that the cells we prospectively isolate as MMP^{high} in the presence of VP are enriched for appropriate signatures of mitochondrial activity. While VP per se and its blocking of efflux pumps may interfere with the steady-state biology of HSCs, these transcriptional assays were conducted at very short time frames, during which no evidence of toxicity or change in cell viability was observed. However, VP's toxicity does interfere with functional studies of HSCs in longer-term studies, and thus we could not directly compare the function of MMP^{high} and MMP^{low} HSCs. Furthermore, mitochondrial dyes themselves can inhibit aspects of mitochondrial function (Perry et al., 2011), and this level of interference may be greater in cells that retain more of the dye. We considered MitoDendra2 reporter mice as an alternative to MMP dyes, but MitoDendra2 is a marker of mitochondrial content and is consequently less useful in aging where MMP is decreased but mass is stable (Figure 1). We have shown here that MMP positively correlates with ATP content and DNA repair capacity of HSCs and negatively correlates with their ROS levels. It will be interesting to understand how MMP relates more broadly to the mitochondrial and metabolic biology of HSCs during aging, particularly in the context of their hypoxic *in vivo* niches; however, a current limitation is the small number of HSCs, which at the moment precludes some of these analyses.

STAR★METHODS

Detailed methods are provided in the online version of this paper and include the following:

SUPPLEMENTAL INFORMATION

Supplemental Information can be found online at https://doi.org/10.1016/j.stem.2020.09.018.

ACKNOWLEDGMENTS

This work was generously funded by grants from the UK (Blood Cancer UK [16001], CHILDREN with CANCER UK, and the Medical Research Council UK [MR/N000838/1]) and Sweden (the Knut and Alice Wallenberg Foundation [500531-1591], The Royal Physiographic Society, Barncancerfonden [PR2019-0099], and VetenskapsRadet [2019-01752]). Mito-Q for drinking water experiments was kindly provided by MitoQ Limited (Auckland, New Zealand). We want to thank Veronika Žemaitė for drawing the graphical abstract. We thank Anna Rydström for sharing the cell-cycle protocol; Parashar Dhapola and Göran Karlsson for providing the CellRadar tool; and Gill May, Rajeev Gupta, and Francisco Iborra for discussions at various stages of this project.

Figure 6. Mito-Q Treatment Can Both Revert and Prevent Onset of the Hematopoietic Aging Phenotype

(A) Schematic diagram of treatment regimen.

(B) Percentage of myeloid ($Mac1/Gr1^+$) cells in PB of individually measured old mice before (pre), in the middle (mid), and at the end of treatment (see Figure 5A) with the range and average (box) percentage change between pre- and end-treatment values (n = 15).

(C) As in (B), but for percentage of B cells ($B220^+$) (n = 15).

(D) Representative histogram of IgM expression in B cells from old (O, purple), young (Y, blue), and old Mito-Q-treated (O+MQ, lilac) mice.

(E) Distribution of myeloid and B cells in PB of old mice (purple) compared to O+MQ mice at the end of a 5-day treatment (lilac) compared to young (blue) mice (n = 12–19).

(F) Sysmex analysis of total white blood cell counts (WBC) and the percentage (Lym%) and absolute number (Lym#) of lymphocytes in old mice at the end of Mito-Q treatment (liliac) compared to young (blue) and old (O) untreated mice (n = 10–15).

(G) Experimental overview.

(H) Left: ratio of myeloid to B cells in MA mice (green) and aged mice kept on normal drinking water (O, purple) compared to mice aged with Mito-Q water (O+MQ, lilac). Right: comparison of PB myeloid, B, and T cells between naturally aged (O, purple) or mice aged with Mito-Q water (O+MQ, lilac) at the endpoint (n = 15, MA; n = 5 O; n = 10 OMQ).

(I) Sysmex whole blood analysis of erythroid parameters of naturally aged (O) or Mito-Q-supplemented (O+MQ) mice (n = 5 O; n = 10 OMQ)

(J) BM analysis of myeloid (M), B cells, and the collective of pre-/pro-B cells (IgM^-B220^+) of naturally aged (O) or Mito-Q-supplemented (O+MQ) mice (n = 5 O; n = 10 OMQ).

(K) Representative FACS plots of erythroid progenitor populations, gated on Lin^- cells ($B220^-$ $Mac1^-$ $Gr1^-$ $CD3^-$) in the BM of naturally aged (O) or Mito-Q-supplemented (O+MQ) mice (see also Figure S6I).

Results are represented as mean ± SEM. *p < 0.05; **p < 0.01; ***p < 0.001; ****p < 0.0001.

AUTHOR CONTRIBUTIONS

E.M. and T.E. conceived the experiments, E.M. and V.S. performed the experiments, and E.D. and J.B. performed the RNA-sequencing. C.J. and S.S. performed the bioinformatics analysis. K.M. and J.L. provided significant feedback on the project. E.M. and T.E. wrote the manuscript. V.S., J.B., E.D., K.M., and J.L. proofread and edited the manuscript.

DECLARATION OF INTERESTS

The authors declare no competing interests.

Received: May 22, 2020
Revised: August 25, 2020
Accepted: September 29, 2020
Published: October 20, 2020

REFERENCES

Akunuru, S., and Geiger, H. (2016). Aging, Clonality, and Rejuvenation of Hematopoietic Stem Cells. Trends Mol. Med. *22*, 701–712.

Baser, A., Skabkin, M., Kleber, S., Dang, Y., Gülcüler Balta, G.S., Kalamakis, G., Göpferich, M., Ibañez, D.C., Schefzik, R., Lopez, A.S., et al. (2019). Onset of differentiation is post-transcriptionally controlled in adult neural stem cells. Nature *566*, 100–104.

Beerman, I., Bhattacharya, D., Zandi, S., Sigvardsson, M., Weissman, I.L., Bryder, D., and Rossi, D.J. (2010). Functionally distinct hematopoietic stem cells modulate hematopoietic lineage potential during aging by a mechanism of clonal expansion. Proc. Natl. Acad. Sci. USA *107*, 5465–5470.

Bonora, M., Ito, K., Morganti, C., Pinton, P., and Ito, K. (2018). Membrane-potential compensation reveals mitochondrial volume expansion during HSC commitment. Exp. Hematol. *68*, 30–37.e1.

Busch, K., and Rodewald, H.R. (2016). Unperturbed vs. post-transplantation hematopoiesis: both in vivo but different. Curr. Opin. Hematol. *23*, 295–303.

Challen, G.A., Boles, N.C., Chambers, S.M., and Goodell, M.A. (2010). Distinct hematopoietic stem cell subtypes are differentially regulated by TGF-beta1. Cell Stem Cell *6*, 265–278.

Chaudhary, P.M., and Roninson, I.B. (1991). Expression and activity of P-glycoprotein, a multidrug efflux pump, in human hematopoietic stem cells. Cell *66*, 85–94.

das Neves, R.P., Jones, N.S., Andreu, L., Gupta, R., Enver, T., and Iborra, F.J. (2010). Connecting variability in global transcription rate to mitochondrial variability. PLoS Biol. *8*, e1000560.

de Almeida, M.J., Luchsinger, L.L., Corrigan, D.J., Williams, L.J., and Snoeck, H.W. (2017). Dye-Independent Methods Reveal Elevated Mitochondrial Mass in Hematopoietic Stem Cells. Cell Stem Cell *21*, 725–729.e4.

de Haan, G., and Lazare, S.S. (2018). Aging of hematopoietic stem cells. Blood *131*, 479–487.

Dykstra, B., Olthof, S., Schreuder, J., Ritsema, M., and de Haan, G. (2011). Clonal analysis reveals multiple functional defects of aged murine hematopoietic stem cells. J. Exp. Med. *208*, 2691–2703.

Grover, A., Sanjuan-Pla, A., Thongjuea, S., Carrelha, J., Giustacchini, A., Gambardella, A., Macaulay, I., Mancini, E., Luis, T.C., Mead, A., et al. (2016). Single-cell RNA sequencing reveals molecular and functional platelet bias of aged haematopoietic stem cells. Nat. Commun. *7*, 11075.

Guantes, R., Rastrojo, A., Neves, R., Lima, A., Aguado, B., and Iborra, F.J. (2015). Global variability in gene expression and alternative splicing is modulated by mitochondrial content. Genome Res. *25*, 633–644.

Gulati, G.S., Zukowska, M., Noh, J.J., Zhang, A., Wesche, D.J., Sinha, R., George, B.M., Weissman, I.L., and Szade, K. (2019). Neogenin-1 distinguishes between myeloid-biased and balanced *Hoxb5*$^{+}$ mouse long-term hematopoietic stem cells. Proc. Natl. Acad. Sci. USA *116*, 25115–25125.

Ito, K., and Suda, T. (2014). Metabolic requirements for the maintenance of self-renewing stem cells. Nat. Rev. Mol. Cell Biol. *15*, 243–256.

Ito, K., Hirao, A., Arai, F., Takubo, K., Matsuoka, S., Miyamoto, K., Ohmura, M., Naka, K., Hosokawa, K., Ikeda, Y., and Suda, T. (2006). Reactive oxygen species act through p38 MAPK to limit the lifespan of hematopoietic stem cells. Nat. Med. *12*, 446–451.

Ito, K., Turcotte, R., Cui, J., Zimmerman, S.E., Pinho, S., Mizoguchi, T., Arai, F., Runnels, J.M., Alt, C., Teruya-Feldstein, J., et al. (2016). Self-renewal of a purified Tie2+ hematopoietic stem cell population relies on mitochondrial clearance. Science *354*, 1156–1160.

Ito, K., Bonora, M., and Ito, K. (2019). Metabolism as master of hematopoietic stem cell fate. Int. J. Hematol. *109*, 18–27.

Jang, Y.Y., and Sharkis, S.J. (2007). A low level of reactive oxygen species selects for primitive hematopoietic stem cells that may reside in the low-oxygenic niche. Blood *110*, 3056–3063.

Jao, C.Y., and Salic, A. (2008). Exploring RNA transcription and turnover in vivo by using click chemistry. Proc. Natl. Acad. Sci. USA *105*, 15779–15784.

Jin, H., Kanthasamy, A., Ghosh, A., Anantharam, V., Kalyanaraman, B., and Kanthasamy, A.G. (2014). Mitochondria-targeted antioxidants for treatment of Parkinson's disease: preclinical and clinical outcomes. Biochim. Biophys. Acta *1842*, 1282–1294.

Kirschner, K., Chandra, T., Kiselev, V., Flores-Santa Cruz, D., Macaulay, I.C., Park, H.J., Li, J., Kent, D.G., Kumar, R., Pask, D.C., et al. (2017). Proliferation Drives Aging-Related Functional Decline in a Subpopulation of the Hematopoietic Stem Cell Compartment. Cell Rep. *19*, 1503–1511.

Kohli, L., and Passegué, E. (2014). Surviving change: the metabolic journey of hematopoietic stem cells. Trends Cell Biol. *24*, 479–487.

Kolb, H.C., Finn, M.G., and Sharpless, K.B. (2001). Click Chemistry: Diverse Chemical Function from a Few Good Reactions. Angew. Chem. Int. Ed. Engl. *40*, 2004–2021.

Kumar, A., and Singh, A. (2015). A review on mitochondrial restorative mechanism of antioxidants in Alzheimer's disease and other neurological conditions. Front. Pharmacol. *6*, 206.

Le, Q., Yao, W., Chen, Y., Yan, B., Liu, C., Yuan, M., Zhou, Y., and Ma, L. (2016). GRK6 regulates ROS response and maintains hematopoietic stem cell self-renewal. Cell Death Dis. *7*, e2478.

Liang, Y., Van Zant, G., and Szilvassy, S.J. (2005). Effects of aging on the homing and engraftment of murine hematopoietic stem and progenitor cells. Blood *106*, 1479–1487.

Liang, R., Arif, T., Kalmykova, S., Kasianov, A., Lin, M., Menon, V., Qiu, J., Bernitz, J.M., Moore, K., Lin, F., et al. (2020). Restraining Lysosomal Activity Preserves Hematopoietic Stem Cell Quiescence and Potency. Cell Stem Cell *26*, 359–376.e7.

Luchsinger, L.L., de Almeida, M.J., Corrigan, D.J., Mumau, M., and Snoeck, H.W. (2016). Mitofusin 2 maintains haematopoietic stem cells with extensive lymphoid potential. Nature *529*, 528–531.

Luchsinger, L.L., Strikoudis, A., Danzl, N.M., Bush, E.C., Finlayson, M.O., Satwani, P., Sykes, M., Yazawa, M., and Snoeck, H.W. (2019). Harnessing Hematopoietic Stem Cell Low Intracellular Calcium Improves Their Maintenance In Vitro. Cell Stem Cell *25*, 225–240.e7.

Matsuzaki, Y., Umemoto, T., Tanaka, Y., Okano, T., and Yamato, M. (2015). β2-Microglobulin is an appropriate reference gene for RT-PCR-based gene expression analysis of hematopoietic stem cells. Regen. Ther. *1*, 91–97.

Montecino-Rodriguez, E., Kong, Y., Casero, D., Rouault, A., Dorshkind, K., and Pioli, P.D. (2019). Lymphoid-Biased Hematopoietic Stem Cells Are Maintained with Age and Efficiently Generate Lymphoid Progeny. Stem Cell Reports *12*, 584–596.

Morganti, C., Bonora, M., Ito, K., and Ito, K. (2019a). Electron transport chain complex II sustains high mitochondrial membrane potential in hematopoietic stem and progenitor cells. Stem Cell Res. (Amst.) *40*, 101573.

Morganti, C., Bonora, M., and Ito, K. (2019b). Improving the Accuracy of Flow Cytometric Assessment of Mitochondrial Membrane Potential in Hematopoietic Stem and Progenitor Cells Through the Inhibition of Efflux Pumps. J. Vis. Exp. (149).

Murphy, M.P., and Smith, R.A. (2007). Targeting antioxidants to mitochondria by conjugation to lipophilic cations. Annu. Rev. Pharmacol. Toxicol. *47*, 629–656.

Nijnik, A., Woodbine, L., Marchetti, C., Dawson, S., Lambe, T., Liu, C., Rodrigues, N.P., Crockford, T.L., Cabuy, E., Vindigni, A., et al. (2007). DNA repair is limiting for haematopoietic stem cells during ageing. Nature *447*, 686–690.

Norddahl, G.L., Pronk, C.J., Wahlestedt, M., Sten, G., Nygren, J.M., Ugale, A., Sigvardsson, M., and Bryder, D. (2011). Accumulating mitochondrial DNA mutations drive premature hematopoietic aging phenotypes distinct from physiological stem cell aging. Cell Stem Cell *8*, 499–510.

Novershtern, N., Subramanian, A., Lawton, L.N., Mak, R.H., Haining, W.N., McConkey, M.E., Habib, N., Yosef, N., Chang, C.Y., Shay, T., et al. (2011). Densely interconnected transcriptional circuits control cell states in human hematopoiesis. Cell *144*, 296–309.

Oguro, H., Ding, L., and Morrison, S.J. (2013). SLAM family markers resolve functionally distinct subpopulations of hematopoietic stem cells and multipotent progenitors. Cell Stem Cell *13*, 102–116.

Orkin, S.H., and Zon, L.I. (2008). Hematopoiesis: an evolving paradigm for stem cell biology. Cell *132*, 631–644.

Pang, W.W., Price, E.A., Sahoo, D., Beerman, I., Maloney, W.J., Rossi, D.J., Schrier, S.L., and Weissman, I.L. (2011). Human bone marrow hematopoietic stem cells are increased in frequency and myeloid-biased with age. Proc. Natl. Acad. Sci. USA *108*, 20012–20017.

Perry, S.W., Norman, J.P., Barbieri, J., Brown, E.B., and Gelbard, H.A. (2011). Mitochondrial membrane potential probes and the proton gradient: a practical usage guide. Biotechniques *50*, 98–115.

Picelli, S., Faridani, O.R., Björklund, A.K., Winberg, G., Sagasser, S., and Sandberg, R. (2014). Full-length RNA-seq from single cells using Smart-seq2. Nat. Protoc. *9*, 171–181.

Ribeiro, R.F., Dabkowski, E.R., Shekar, K.C., O Connell, K.A., Hecker, P.A., and Murphy, M.P. (2018). MitoQ improves mitochondrial dysfunction in heart failure induced by pressure overload. Free Radic. Biol. Med. *117*, 18–29.

Rimmelé, P., Liang, R., Bigarella, C.L., Kocabas, F., Xie, J., Serasinghe, M.N., Chipuk, J., Sadek, H., Zhang, C.C., and Ghaffari, S. (2015). Mitochondrial metabolism in hematopoietic stem cells requires functional FOXO3. EMBO Rep. *16*, 1164–1176.

Rodriguez-Fraticelli, A.E., Wolock, S.L., Weinreb, C.S., Panero, R., Patel, S.H., Jankovic, M., Sun, J., Calogero, R.A., Klein, A.M., and Camargo, F.D. (2018). Clonal analysis of lineage fate in native haematopoiesis. Nature *553*, 212–216.

Rossi, D.J., Bryder, D., Zahn, J.M., Ahlenius, H., Sonu, R., Wagers, A.J., and Weissman, I.L. (2005). Cell intrinsic alterations underlie hematopoietic stem cell aging. Proc. Natl. Acad. Sci. USA *102*, 9194–9199.

Rossi, D.J., Bryder, D., Seita, J., Nussenzweig, A., Hoeijmakers, J., and Weissman, I.L. (2007). Deficiencies in DNA damage repair limit the function of haematopoietic stem cells with age. Nature *447*, 725–729.

Rossman, M.J., Santos-Parker, J.R., Steward, C.A.C., Bispham, N.Z., Cuevas, L.M., Rosenberg, H.L., Woodward, K.A., Chonchol, M., Gioscia-Ryan, R.A., Murphy, M.P., and Seals, D.R. (2018). Chronic Supplementation With a Mitochondrial Antioxidant (MitoQ) Improves Vascular Function in Healthy Older Adults. Hypertension *71*, 1056–1063.

Säwen, P., Eldeeb, M., Erlandsson, E., Kristiansen, T.A., Laterza, C., Kokaia, Z., Karlsson, G., Yuan, J., Soneji, S., Mandal, P.K., et al. (2018). Murine HSCs contribute actively to native hematopoiesis but with reduced differentiation capacity upon aging. eLife *7*, e41258.

Signer, R.A., Magee, J.A., Salic, A., and Morrison, S.J. (2014). Haematopoietic stem cells require a highly regulated protein synthesis rate. Nature *509*, 49–54.

Sigurdsson, V., Takei, H., Soboleva, S., Radulovic, V., Galeev, R., Siva, K., Leeb-Lundberg, L.M., Iida, T., Nittono, H., and Miharada, K. (2016). Bile Acids Protect Expanding Hematopoietic Stem Cells from Unfolded Protein Stress in Fetal Liver. Cell Stem Cell *18*, 522–532.

Simsek, T., Kocabas, F., Zheng, J., Deberardinis, R.J., Mahmoud, A.I., Olson, E.N., Schneider, J.W., Zhang, C.C., and Sadek, H.A. (2010). The distinct metabolic profile of hematopoietic stem cells reflects their location in a hypoxic niche. Cell Stem Cell *7*, 380–390.

Snoeck, H.W. (2017). Mitochondrial regulation of hematopoietic stem cells. Curr. Opin. Cell Biol. *49*, 91–98.

Subramanian, A., Tamayo, P., Mootha, V.K., Mukherjee, S., Ebert, B.L., Gillette, M.A., Paulovich, A., Pomeroy, S.L., Golub, T.R., Lander, E.S., and Mesirov, J.P. (2005). Gene set enrichment analysis: a knowledge-based approach for interpreting genome-wide expression profiles. Proc. Natl. Acad. Sci. USA *102*, 15545–15550.

Sudo, K., Ema, H., Morita, Y., and Nakauchi, H. (2000). Age-associated characteristics of murine hematopoietic stem cells. J. Exp. Med. *192*, 1273–1280.

Sukumar, M., Liu, J., Mehta, G.U., Patel, S.J., Roychoudhuri, R., Crompton, J.G., Klebanoff, C.A., Ji, Y., Li, P., Yu, Z., et al. (2016). Mitochondrial Membrane Potential Identifies Cells with Enhanced Stemness for Cellular Therapy. Cell Metab. *23*, 63–76.

Szilvassy, S.J., Humphries, R.K., Lansdorp, P.M., Eaves, A.C., and Eaves, C.J. (1990). Quantitative assay for totipotent reconstituting hematopoietic stem cells by a competitive repopulation strategy. Proc. Natl. Acad. Sci. USA *87*, 8736–8740.

Takihara, Y., Nakamura-Ishizu, A., Tan, D.Q., Fukuda, M., Matsumura, T., Endoh, M., Arima, Y., Chin, D.W.L., Umemoto, T., Hashimoto, M., et al. (2019). High mitochondrial mass is associated with reconstitution capacity and quiescence of hematopoietic stem cells. Blood Adv. *3*, 2323–2327.

Till, J.E., and McCulloch, E.A. (1961). A direct measurement of the radiation sensitivity of normal mouse bone marrow cells. Radiat. Res. *14*, 213–222.

Umemoto, T., Hashimoto, M., Matsumura, T., Nakamura-Ishizu, A., and Suda, T. (2018). Ca^{2+}-mitochondria axis drives cell division in hematopoietic stem cells. J. Exp. Med. *215*, 2097–2113.

Vannini, N., Girotra, M., Naveiras, O., Nikitin, G., Campos, V., Giger, S., Roch, A., Auwerx, J., and Lutolf, M.P. (2016). Specification of haematopoietic stem cell fate via modulation of mitochondrial activity. Nat. Commun. *7*, 13125.

Wahlestedt, M., Erlandsson, E., Kristiansen, T., Lu, R., Brakebusch, C., Weissman, I.L., Yuan, J., Martin-Gonzalez, J., and Bryder, D. (2017). Clonal reversal of ageing-associated stem cell lineage bias via a pluripotent intermediate. Nat. Commun. *8*, 14533.

White, M.C., Holman, D.M., Boehm, J.E., Peipins, L.A., Grossman, M., and Henley, S.J. (2014). Age and cancer risk: a potentially modifiable relationship. Am. J. Prev. Med. *46* (3, Suppl 1), S7–S15.

Zorova, L.D., Popkov, V.A., Plotnikov, E.Y., Silachev, D.N., Pevzner, I.B., Jankauskas, S.S., Babenko, V.A., Zorov, S.D., Balakireva, A.V., Juhaszova, M., et al. (2018). Mitochondrial membrane potential. Anal. Biochem. *552*, 50–59.

Please cite this article in press as: Mansell et al., Mitochondrial Potentiation Ameliorates Age-Related Heterogeneity in Hematopoietic Stem Cell Function, Cell Stem Cell (2020), https://doi.org/10.1016/j.stem.2020.09.018

STAR★METHODS

KEY RESOURCES TABLE

REAGENT or RESOURCE	SOURCE	IDENTIFIER
Antibodies		
PE/Cy5 anti-mouse TER-119	BioLegend	Cat#116210; RRID: AB_313711
PE/Cy5 anti-mouse Ly-6G/Ly-6C (Gr-1); RB6-8C5	BioLegend	Cat#108410; RRID: AB_313375
PE/Cy5 anti-mouse/human CD45R/B220; RA3-6B2	BioLegend	Cat#103210; RRID: AB_312995
PE/Cy5 anti-mouse CD3e; 145-2C11	BioLegend	Cat#100310; RRID: AB_312675
PE/Cy5 anti-mouse/human CD11b; M1/70	BioLegend	Cat#101210; RRID: AB_312793
APC-eFluor 780 anti-mouse CD117 (c-Kit); 2B8	Invitrogen (eBioscience)	Cat#47-1171-82; RRID: AB_1272177
Brilliant Violet 421 anti-mouse Ly-6A/E (Sca-1); D7	BioLegend	Cat#108128; RRID: AB_2563064
PE/Cy7 anti-mouse CD48; HM48-1	BioLegend	Cat#103424; RRID: AB_2075049
Brilliant Violet 605 anti-mouse CD150 (SLAM); TC15-12F12.2	BioLegend	Cat#115927; RRID: AB_11204248
Brilliant Violet 605 anti-mouse CD45.1; A20	BioLegend	Cat#110738; RRID: AB_2562565
PE anti-mouse CD45.2; 104	BioLegend	Cat#109807; RRID: AB_313444
PE anti-mouse IgM; RMM-1	BioLegend	Cat#406508; RRID: AB_315058
PE anti-mouse CD45.1; A20	BioLegend	Cat#110708; RRID: AB_313497
PE anti-mouse Ly-6A/E (Sca-1); E13-161.7	BioLegend	Cat#122508; RRID: AB_756193
APC anti-mouse CD3e; 145-2C11	BioLegend	Cat#100312; RRID: AB_312677
APC anti-mouse/human CD45R/B220; RA3-6B2	BioLegend	Cat#103212; RRID: AB_312997
APC anti-mouse CD48; HM48-1	BioLegend	Cat#103412; RRID: AB_571997
APC anti-mouse CD45.2; 104	BioLegend	Cat#109814; RRID: AB_389211
APC anti-mouse Ly-6G/Ly-6C (Gr-1); RB6-8C5	BioLegend	Cat#108412; RRID: AB_313377
APC anti-mouse/human CD11b; M1/70	BioLegend	Cat#101212; RRID: AB_312795
APC anti-mouse CD117 (c-Kit); 2B8	BioLegend	Cat#105812; RRID: AB_313221
APC/Cyanine7 anti-mouse CD45.2; 104	Biolegend	Cat#109824; RRID: AB_830789
FITC hamster anti-mouse CD3e; 145-2C11	BD Biosciences	Cat#553062; RRID: AB_394595
FITC rat anti-mouse CD4; H129.19	BD Biosciences	Cat#553651; RRID: AB_394971
FITC anti-mouse CD48; HM48-1	BioLegend	Cat#103403; RRID: AB_313018
FITC anti-mouse CD45.1; A20	BioLegend	Cat#110706; RRID: AB_313495
FITC anti-mouse CD71; RI7217	BioLegend	Cat#113806; RRID: AB_313567
PerCP rat anti-mouse CD8a; 53-6.7	BD Biosciences	Cat#553036; RRID: AB_394573
PE/Cy7 anti-mouse TER119	eBioscience	Cat#25-5921-82; RRID: AB_469661
PE/Cy7 anti-mouse CD150; TC15-12F12.2	BioLegend	Cat#115914; RRID: AB_439797
PE/Cy7 anti-mouse CD45.1; A20	BioLegend	Cat#110730; RRID: AB_1134168
BV421 Rat Anti-Mouse CD135; A2F10.1	BD Biosciences	Cat#562898; RRID: AB_2737876
PE anti-mouse CD127 (IL-7Rα); A7R34	BioLegend	Cat#135010; RRID: AB_1937251
Zombie Red Fixable Viability dye	BioLegend	Cat#423109
FITC anti-H2A.X Phospho (Ser139); 2F3	BioLegend	Cat#613404; RRID: AB_528919
Chemicals, Peptides, and Recombinant Proteins		
Ammonium Chloride Solution	STEMCELL technologies	Cat#07800
4',6-diamidino-2-phenylindole (DAPI)	ThermoFischer	Cat#D1306
5-ethynyl uridine (5-EU)	ThermoFischer	Cat# E10345

(*Continued on next page*)

Continued

REAGENT or RESOURCE	SOURCE	IDENTIFIER
o-propargyl puromycin (OPP)	Jena Bioscience	Cat#Nu-931-5
Mitoquinol (for injection)	Cayman Chemicals	Cat# 89950
Mitoquonol (for drinking water supplementation)	MitoQ Limited	gifted
CCCP	Sigma Aldrich	Cat# C2759
5,6-Dichlorobenzimidazole 1-β-D-ribofuranoside (DRB)	Sigma Aldrich	Cat# D1916
Actinomycin-D	Sigma Aldrich	Cat# A1410
Flavopiridol	Sigma Aldrich	Cat# F3055
Verapamil	Sigma Aldrich	Cat# V4629
Tetramethylrhodamine, Methyl Ester, Perchlorate (TMRM)	ThermoFischer	Cat# I34361
Tetramethylrhodamine, Ethyl Ester, Perchlorate (TMRE)	ThermoFischer	Cat# T669
1,1′,3,3,3′,3′-hexamethylindodicarbocyanine iodide (DilC1(5))	ThermoFischer	Cat# M34151
Mitotracker Green	ThermoFischer	Cat# M7514
JC-1	ThermoFischer	Cat#M34152
Critical Commercial Assays		
FITC anti-mouse Ki-67 kit	BD PharMingen	Cat#556026
CD117 Microbeads, mouse	Miltenyi Biotec	Cat#130-091-224
Click-iT RNA Alexa Fluor 488 Imaging Kit	ThermoFischer	Cat#C10329
Click-iT Plus OPP Alexa Fluor 488 Protein Synthesis Assay Kit	ThermoFischer	Cat#C10456
DCFDA/H2DCFDA- Cellular ROS Assay Kit	Abcam	Cat#ab113851
Luminescent ATP Detection Assay Kit	Abcam	Cat#ab113849
MitoSOX Red Mitochondrial Superoxide Indicator	N/A	Cat#M36008
RNeasy Micro Kit	QIAGEN	Cat#74004
Agencourt AMPureXP magnetic beads	Beckman Coulter	Cat#A63881
Bioanalyser high sensitivity DNA chip	Agilent	Cat#5067-4626
Bioanalyser RNA 6000 Pico chip	Agilent	Cat#5067-1513
Qubit High Sensitivity DNA kit	ThermoFisher	Cat#Q32851
Nextera XT DNA Preparation Kit	Illumina	Cat# FC-131-1096
NextSeq500/550 High Output Kit v2.5	Illumina	Cat#20024908
Deposited Data		
RNA seq #1 (Figures 3 and S3)	This paper	GEO: GSE156805
RNA seq #2 (Figures 4 and S4)	This paper	GEO: GSE156807
Experimental Models: Organisms/Strains		
C57BL/6 JRj mice	Janvier	RRID: MGI:2670020
C57BL/6 NRj mice	Janvier	RRID:MGI:6236253
C57BL/6 x B6.SJL mice	In house	N/A
B6.SJL	In house	N/A
Oligonucleotides		
See Table S1		
Software and Algorithms		
GSEA	Broad Institute	https://www.gsea-msigdb.org/gsea/index.jsp
CellRadar	Dhapola et al., personal communication	https://karlssong.github.io/cellradar/
Flowjo v10	BD	https://www.flowjo.com

(*Continued on next page*)

Continued

REAGENT or RESOURCE	SOURCE	IDENTIFIER
FACSDiva	BD	https://www.bdbiosciences.com/en-us/instruments/research-instruments/research-software/flow-cytometry-acquisition/facsdiva-software
Prism v7.0c	Graphpad	https://www.graphpad.com/scientific-software/prism/
DAVID Bioinformatics Resources v6.8	LHRI	https://david.ncifcrf.gov/home.jsp
Other		
DPBS/modified calcium, magnesium free	HyClone	Cat#SH30028.02
Penicillin-Streptomycin 100X solution	HyClone	Cat#SV30010
StemSpan SFEM	STEMCELL technologies	Cat#09650

RESOURCE AVAILABILITY

Lead Contact

Further information and requests for resources or reagents should be directed to and will be fulfilled by the Lead Contact, Tariq Enver (t.enver@ucl.ac.uk).

Materials Availability

This study did not generate new materials or reagents.

Data and Code Availability

RNA-seq data are available at NCBI GEO with the following reference series: GSE156808 and accession numbers: GSE156805 and GSE156807.

EXPERIMENTAL MODEL AND SUBJECT DETAILS

Mice

Young adult (8-16 weeks) and Aged (18-24 months) C56Bl/6Jrj mice (CD45.2), as well as young (8-16 weeks) C56Bl/6Nrj mice (CD45.2) were purchased from Janvier Labs. Aged mice were analyzed at 18-20 months of age, unless indicated otherwise. B6.SJL (CD45.1) mice and C56Bl/6 x B6.SJL mice (CD45.1/CD45.2) used for transplantation experiments were generated in house. Mice were housed in plastic cages in a controlled environment with 12-hour light-dark cycles and chow and water were provided *ad libitum*. Experiments and animal care were performed in accordance with the Lund University Animal Ethical Committee.

METHOD DETAILS

Peripheral Blood analysis

PB was collected from the tail vein into EDTA-coated microvette tubes (Sarstedt Cat# 20.1341.100) and placed on a roller to prevent coagulation. Whole blood count analysis was performed using an automated hematology analyzer (Sysmex KX-21N). For FACS analysis, PB was lysed in ammonium chloride solution (STEMCELL technologies) for 10 min at room temperature and washed twice prior to staining for cell surface markers for 45 min at 4°C in the dark. Cells were washed in FACS buffer (PBS+2%FBS) and filtered prior to flow cytometric analysis.

Bone Marrow analysis

Mice were euthanised by spinal dislocation followed by the dissection of the spinal bones and both right and left femurs, tibias and iliacs. Bones were crushed using a pestle and mortar and bone marrow cells were collected in 20 mL ice-cold FACS buffer (PBS+2% FBS), filtered and washed (350x*g*, 5 min). BM cells were either c-kit enriched using CD117 beads and magnetic separation (MACS Miltenyi Biotec, according to manufacturer's instructions) when progenitor populations were analyzed, or simply lysed for red blood cells (ammonium chloride solution, STEMCELL technologies) for 10 min at room temperature, when mature populations were analyzed. Cells were washed and stained for cell surface markers for 45 min at 4°C in the dark. Cells were washed in FACS buffer and filtered prior to FACS sorting or flow cytometric analysis.

FACS sorting and analysis

For HSC sorting, bone marrow was c-Kit enriched and stained for HSC-SLAM cell surface markers (Lineage (B220, CD3e, Ter119, Mac1, Gr1), cKit (CD117), Sca1, CD48, CD150, see table for antibody specification), washed, filtered and kept on ice as single cell

Please cite this article in press as: Mansell et al., Mitochondrial Potentiation Ameliorates Age-Related Heterogeneity in Hematopoietic Stem Cell Function, Cell Stem Cell (2020), https://doi.org/10.1016/j.stem.2020.09.018

suspension in FACS buffer (PBS+ 2%FBS). Prior to analysis or sorting, 7AAD was added to allow for dead cell exclusion. FACS sorting was performed on a FACS Aria-III or Aria-IIu machine (BD). FACS analysis that did not require cell sorting was performed on LSR FORTESSA (BD) or FACS LSRII (BD). All machines are running FACS Diva software (BD). Final analysis, including generation of FACS plots and histograms, was performed using FlowJo software v.10 (BD).

Metabolic analyses

Mitochondrial membrane potential and mass

After cell surface staining, cells were washed and incubated for 20-30 min at 37°C suspended in 1mL FACS buffer (PBS+2%FBS) with either of these mitochondrial dyes: Mitotracker Green (30nM, MTG, ThermoFisher) TMRM (100nM, ThermoFisher), TMRE (100nM, ThermoFisher), DilC1(5) (50nM, ThermoFisher) or JC-1 (2uM, ThermoFisher) according to manufacturer's instructions, together with verapamil (50uM, dissolved in PBS from an original 10mg/ml stock solution in DMSO, Sigma-Aldrich #V4629) unless stated otherwise. Cells were washed twice (400x*g*, 5 min) and analyzed by Flow Cytometry. Dye sensitivity of all dyes at the used concentrations was validated by measuring dye fluorescence after mitochondrial uncoupling (CCCP at 30uM for 30 min prior to MMP staining).

ATP content

Intracellular ATP content was measured using the Luminescent ATP Detection Assay Kit (Abcam, Cat#ab113849) according to manufacturer's instructions. In brief, 1000 MMP^{high} or MMP^{low} HSCs were FACS sorted into single wells of a 96-well special optics plate (Costar, Cat#3615) in 100uL FACS buffer (PBS+2%FBS). Then 50 μL detergent was added to samples followed by a 5 min incubation in an orbital shaker at 600-700 rpm protected from light, for cell lysis and stabilization of ATP. Then 50uL of substrate solution was added followed by a 5 min incubation in an orbital shaker at 600-700 rpm protected from light. The plate was dark-adapted by covering for 10 min followed by measurements of luminescence using a GloMax® Discover microplate reader (Promega).

ROS and mitochondrial superoxide

Intracellular ROS levels were measured by FACS following cell surface staining, using the DCFDA/H2DCFDA kit (Abcam, Cat#ab113851) according to manufacturer's instructions. Cells were stained with 20uM DCFDA in 1X buffer for 30 min at 37°C, washed in 1X buffer and analyzed by Flow Cytometry. Verapamil inclusion in this staining resulted in significantly reduced levels of dye fluorescence across bone marrow lineages including HSCs (data not shown) and therefore verapamilVP was not included in this staining. Dye sensitivity at this concentration was validated by measuring dye fluorescence after tert-butyl hydrogren peroxide (TBHP) exposure which readily increases DCFDA signal.

Mitochondrial superoxide was measured by FACS following cell surface staining using MitoSOX Red Mitochondrial Superoxide Indicator (ThermoFisher, Cat#M36008). Cells were stained with MitoSox (5uM) for 30 min at 37°C together with verapamilVP (50uM, dissolved in PBS from an original 10mg/ml stock solution in DMSO, Sigma-Aldrich #V4629). In absence of verapamil, MitoSox dye was disproportionally effluxed in HSPCs including HSCs relative to mature BM populations (data not shown) and therefore verapamil was included in this staining. Dye sensitivity at this concentration was validated by measuring dye fluorescence after tert-butyl hydrogren peroxide (TBHP) exposure which readily increases MitoSox signal.

Transcription/Translation rate analysis

Global transcription rate was measured *in vivo* through Click-iT detection of incorporation of labeled nucleotide over a specific period of time (Jao and Salic, 2008). In brief, mice were intraperitoneally injected with 0.5 mg alkyne-labeled 5-ethynyl uridine (5-EU; ThermoFisher, Cat# E10345) which readily incorporates into nascent RNA. Titration of 5-EU was done to ensure signal saturation in all BM lineages at the injected dose (Figure S2A). Mice were sacrificed one hour later after which BM was harvested and stained for cell surface markers. Cells were fixed and permeabilised (Cytofix/Cytoperm, BD, Cat# 554714) for 20 min at 4°C, washed in 1X perm/wash buffer (BD) in dH2O, followed by click-it reaction for 30 min at RT protected from light according to manufacturer's instructions (Click-iT RNA Alexa Fluor 488 Imaging Kit, ThermoFisher Cat#C10329) in which azide-labeled fluorophore AF-488 is 'clicked' to the alkyne-labeled 5-EU, allowing for flow cytometric detection. The click-it reaction occurred in presence of copper protectant (ThermoFisher Cat#C10641) at a volume ratio of 3:2 with the copper sulfate (CuS04) component to protect fluorescence of PE and PE-conjugated dyes used in the cell surface stain. Cells were washed in reaction buffer rinse provided in the Click-iT kit, filtered and analyzed by FACS. Similarly, for analysis of protein translation rate, Click-iT detection of alkyne-labeled o-propargyl puromycin (OPP, Jena Bioscience, Cat#Nu-931-5) incorporation into nascent peptide was measured 45 min after intraperitoneal injection of 0.5mg and analyzed by FACS after conjugation with azide-labeled fluorophore (ThermoFisher, Cat#C10456).

Transcription rate in cells sorted on MMP

To circumvent the incompatibility of the Click-iT protocol which requires fixation and permeabilisation with the staining for MTG, TMRM or DilC1(5) whose signal is not retained upon fixation, a two-step protocol was used. Cells were FACS sorted based on 30% highest or lowest MMP after *in vivo* incubation with labeled 5-EU. MMP^{high} or MMP^{low} sorted cells were then fixed, permeabilised, followed by a Click-iT reaction to label the incorporated 5-EU and re-analyzed by FACS to measure transcriptional rate in relation to MMP.

Cell cycle Analysis

Following cell surface staining, cells were fixed for 30 min at 4°C followed by a wash with wash/perm solution (Cytofix/Cytoperm, BD, Cat# 554714) and spun down at 500x*g* for 5min. Cells were then incubated in 200uL 0.25% Triton X-100 (diluted in wash/perm so-

lution) for 60min at 4°C, washed (500x*g* for 5min) and stained with Fitc-Ki-67 (1:100 concentration in wash/perm solution) and stained for 60min at 4°C, and washed. Cell concentration was kept below 2x10^6/ml. DAPI was added at a final concentration of ~1ug/ml (or ~$5*10^{-13}$g/cell); any sub-dilution was made in H2O). Cells were analyzed by FACS (LSRII; BD), on low flow rate ensuring that acquisition rate always remained below 1000 events/s.

DNA damage analysis

DNA double strand breaks were measured using staining for y-H2AX (phosphorylation of Ser139 of H2A histone family member X which occurs upon DNA double strand breaks) followed by FACS analysis, either at steady state or after irradiation. Mice received a 2Gy single dose of irradiation and the femur and tibia were harvested 30min, 1 hr, 2 hr or 4 hr later. We first validated that y-H2AX staining in young HSCs peaks at 30 min- 1 hr after a single dose of 2Gy irradiation and recovers to pre-irradiation levels around 4 hr post-irradiation (data not shown), and therefore y-H2AX was subsequently measured at 30 min- 1 hr after irradiation. For y-H2AX detection, BM cells were stained using conventional SLAM markers (LSK $CD48^{-}CD150^{+}$) before they were fixed using the BD Fix/Perm kit (Cytofix/Cytoperm, BD, Cat# 554714) for 30 min. Cells were subsequently permeabilised using the BD Fix/Perm solution + 0,25% of Triton X-100 for 30 min followed by incubation with y-HA2X antibody (Abcam, 5uL per 100ul, according to manufacturer's instructions) for 30 min. Cells were then stained with Zombie Red Fixable Viability dye (Biolegend, according to manufacturer's instructions) to allow for dead cell exclusion. Samples were analyzed and data collected using LSRII flow cytometer.

Chemical treatment of mice

Mitoquinol was either administered through intra-peritoneal injection (2 mg/kg body weight, Cayman Cat# 89950) or administered orally through drinking water supplementation (350 mM (kindly provided by MitoQ Limited) dissolved in sucrose-supplemented water (5g/L) which was given to both the Mito-Q and the control group.

Carbonyl cyanide 3-chloropheylhydrazone (CCCP; 0.3-1.0 mg/kg bw, Sigma), Actinomycin-D (0.1-1.0 mg/kg bw, Flavopiridol (0.5-5.0 mg/kg bw) and 5,6-Dichlorobenzimidazole 1-β-D-ribofuranoside (DRB; 1-10 mg/kg bw) were administered through single intraperitoneal injection. All chemicals were administered in 200uL PBS (with < 10% DMSO when initial stock solutions were prepared in DMSO).

Mito-Q treatment *in vitro*

Short-term (2 hr) *in vitro* treatment with Mito-Q was performed to directly assess the impact of Mito-Q on MMP and DNA damage repair in HSCs from old mice.

For assessment of DNA damage repair, bone marrow cells were harvested 1 hr after mice were exposed to 2Gy of irradiation. cKit-enriched cells were then seeded in 48-well plates at a concentration of $5*10^5$ cells/well in 150 uL of StemSpan SFEM (STEMCELL technologies) supplemented with 1% Penicillin/Streptomycin (HyClone), with or without Mito-Q at 0.5, 1, 2, 4 or 8 uM concentrations, for a 2 hr incubation at 37°C. Cells were then washed, stained for cell surface antibodies followed by staining DNA damage marker y-H2AX.

A similar protocol was used for assessment of MMP after short-term (2hr) *in vitro* treatment with Mito-Q, albeit cells were harvested from old mice at steady state in absence of irradiation insult.

RT-PCR gene expression analysis

For real-time quantitative polymerase chain reaction (RT-qPCR), cells were sorted into 350uL RLT lysis buffer (QIAGEN) and total RNA was isolated (RNeasy Micro, QIAGEN) according to manufacturer's instructions. cDNA was prepared through reversed transcription (Superscript III First Strand Synthesis kit, Invitrogen) using a T100 thermal cycler (BioRad). qRT-PCR analysis was performed using Taqman gene expression mastermix (ThermoFisher Cat#4369016) and primers (Taqman real-time PCR primers (FAM), see resource table for primer specifications) on a 7900HT Fast Real-Time PCR system (IScience). Gene expression was normalized to *B2m* expression (Matsuzaki et al., 2015).

RNA sequencing (low cell number bulk)

HSCs (1000 per sample) were sorted directly into 800 μL TRIzol Reagent® (ThermoFisher, Cat#15596018) and frozen at −80°C. Total RNA was extracted from the aqueous phase after addition of 200 μL chloroform and precipitated by mixing an equal volume of isopropanol supplemented with 5 μg of linear polyacrylamide (Sigma). The RNA pellet was washed twice with fresh 80% ethanol and resuspended in 5 μL RNase-free water. 1 μL of RNA was quantified on an Agilent Bioanalyser RNA 6000 Pico chip. 100pg of RNA were used to generate cDNA using a modified Smart-seq2 protocol (Picelli et al., 2014). cDNA was amplified using SeqAmp Polymerase (Takara) and 16 cycles at thermal conditions recommended by the manufacturer. The resulting cDNA libraries were purified with Agencourt AMPureXP magnetic beads (0.8 to 1 beads to cDNA ratio), washed twice with fresh 80% ethanol and eluted in 15 μL EB buffer. 1 μL cDNA was quality checked on an Agilent Bioanalyser high sensitivity DNA chip and quantified using Qubit High Sensitivity DNA kit (Thermo Fisher, Cat# Q32851). Sequencing libraries were produced from the cDNA libraries using Nextera XT DNA Preparation Kit (Illumina) following a modified version of the manufacturer's protocol with 20-fold volume reduction (2.5 μL final volume). 50pg of cDNA were tagmented followed by 13 cycles of amplification. Equimolar amounts of each sequencing library were ascertained and pooled using the Echo 525 liquid handler (Labcyte). Pool was purified with 0.8x Agencourt AMPureXP magnetic beads, eluted in 25 μL EB buffer, quality checked on an Agilent Bioanalyser high sensitivity DNA chip and quantified using Qubit High

Sensitivity DNA kit. Pool was diluted to a final concentration of 2pM and sequenced on the Illumina NextSeq 500 platform using NextSeq500/550 High Output Kit v2.5 (2x76 paired end cycles).

Differential Gene Expression Analysis

Raw reads were quality controlled and trimmed using Trim Galore (https://www.bioinformatics.babraham.ac.uk/projects/trim_galore/) prior to mapping using STAR v2.7 against the mouse GRCm38.95 assembly. Gene counts were produced using QoRTs (26187896) after which duplicates were managed using Markduplicates from Picard v4.0.1.1 (https://broadinstitute.github.io/picard/) and DupRadar (27769170). Samples were clustered using the hclust function for R using correlation distance, and differentially expressed genes were identified using DESeq2 (25516281).

Gene Set Enrichment Analysis was performed (Subramanian et al., 2005), computing overlap with our complete raw dataset and MSigDB gene sets provided by the software (Hallmark and KEGG), as well as published gene sets: MitoCarta2.0 (Broad Institute) and Novershtern et al. (2011).

Gene ontology analysis was performed by computing overlap between our differentially expressed gene sets and known gene ontology signatures using DAVID Bioinformatics Resources v6.8 (Laboratory of Human Retrovirology and Immunoinformatics (LHRI)).

CellRadar

Visualization of the differentially expressed gene was performed using software CellRadar (https://karlssong.github.io/cellradar/); developed by the G. Karlsson lab, Lund University, (Parashar Dhapola et al., personal communication) based on normalized gene expression data from normal human hematopoiesis (HemaExplorer) from the Bloodspot database (http://servers.binf.ku.dk/bloodspot/).

Transplantation assays

Recipient mice were lethally irradiated (900cGY) 6-12 hr prior to transplantation. Isolated HSCs from young (100 HSCs) and old mice (300 HSCs), together with 200.000 whole BM support cells were transplanted in 350uL FACS buffer (PBS+2%FBS) through intravenous tail vein injection. Drinking water of recipient mice was supplemented with ciprofloxacin (125mg/L, HEXAL) for 3 weeks to prevent infection during this period of myelo-ablation. Peripheral blood was analyzed for donor engraftment and lineage kinetics at weeks 3, 4, 6, 10 and 16 after transplantation. Bone marrow engraftment, lineage kinetics and MMP status were analyzed at the 16-week endpoint.

QUANTIFICATION AND STATISTICAL ANALYSIS

Statistical analysis was performed in Graphpad Prism 7. Results are represented as mean ± SEM. The number of experimental subjects per experiment is given (n =) and these are generated from 2, 3 or 4 independently repeated experiments unless otherwise stated. When comparing more than 2 groups, ANOVA was performed with post hoc Tukey correction for multiple comparisons. When ANOVA showed significant difference ($p < 0.05$), multiple comparison analysis was performed using unpaired Student's t test, unless otherwise stated. When only 2 groups were compared, an unpaired Student's t test was used, unless otherwise stated. Statistical significance is indicated in figures as follows: *$p < 0.05$; **$p < 0.01$; ***$p < 0.001$; ****$p < 0.0001$. In bulk RNA-sequencing analysis, differentially expressed genes are defined as having a greater than 2-fold change in expression and a false discovery rate below 5% (Figures 3 and S3) or below 10% (Figures 4 and S4).